NASA TECHNICAL NOTE

NASA TN D-7701

NASA TN D-7701

USE OF HEXAFLUOROETHANE TO SIMULATE THE INVISCID REAL-GAS EFFECTS ON BLUNT ENTRY VEHICLES

by James L. Hunt, Robert A. Jones, and Kathryn A. Smith

Langley Research Center
Hampton, Va. 23665

NATIONAL AERONAUTICS AND SPACE ADMINISTRATION • WASHINGTON, D. C. • OCTOBER 1974

1. Report No.	2. Government Accession No.	3. Recipient's Catalog No.
NASA TN D-7701		

4. Title and Subtitle	5. Report Date
USE OF HEXAFLUOROETHANE TO SIMULATE THE INVISCID REAL-GAS EFFECTS ON BLUNT ENTRY VEHICLES	October 1974
	6. Performing Organization Code
7. Author(s)	8. Performing Organization Report No.
James L Hunt, Robert A. Jones, and Kathryn A. Smith	L-9459
	10. Work Unit No.
9. Performing Organization Name and Address	760-66-01-02
NASA Langley Research Center Hampton, Va. 23665	11. Contract or Grant No.
	13. Type of Report and Period Covered
12. Sponsoring Agency Name and Address	Technical Note
National Aeronautics and Space Administration Washington, D.C. 20546	14 Sponsoring Agency Code

15. Supplementary Notes

16. Abstract

Results are presented of an experimental and theoretical investigation of the use of equilibrium hexafluoroethane (C_2F_6) as an undissociated test gas in a wind tunnel to simulate the inviscid aerodynamic characteristics of blunt bodies in high-speed flight where dissociation occurs. The results indicate that the use of C_2F_6 as a test gas in wind tunnels is a practical and relatively simple and inexpensive method of obtaining test conditions with large normal-shock density ratios which is the necessary condition for blunt-body inviscid similitude. Equations for the thermodynamic and transport properties of C_2F_6 are also included.

17. Key Words (Suggested by Author(s))	18. Distribution Statement
Real-gas effects Blunt body Hexafluoroethane Inviscid flow field	Unclassified – Unlimited STAR Category 12

19. Security Classif. (of this report)	20. Security Classif. (of this page)	21. No. of Pages	22. Price*
Unclassified	Unclassified	44	$3.25

*For sale by the National Technical Information Service, Springfield, Virginia 22151

USE OF HEXAFLUOROETHANE TO SIMULATE THE INVISCID REAL-GAS EFFECTS ON BLUNT ENTRY VEHICLES

By James L. Hunt, Robert A. Jones, and Kathryn A. Smith
Langley Research Center

SUMMARY

Results are presented of an experimental and theoretical investigation of the use of equilibrium hexafluoroethane (C_2F_6) as an undissociated test gas in a wind tunnel to simulate the inviscid aerodynamic characteristics of blunt bodies in high-speed flight where dissociation occurs. The results indicate that the use of C_2F_6 as a test gas in wind tunnels is a practical and relatively simple and inexpensive method of obtaining test conditions with large normal-shock density ratios which is the necessary condition for blunt-body inviscid similitude. Equations for the thermodynamic and transport properties of C_2F_6 are also included.

INTRODUCTION

A study was made in reference 1 of the simulation of reentry conditions which can be obtained in ground test facilities. This study concluded that the high Mach number, high-enthalpy characteristics of reentry conditions were not duplicated in operational ground facilities. These high-enthalpy conditions result in highly compressible real-gas flows. As a blunt body enters a planetary atmosphere at hypersonic speeds, the gas molecules that pass through the bow shock are excited to higher vibrational and chemical energy modes. This lowers the specific-heat ratio of the gas below the free-stream value, if it is assumed that equilibrium exists and provided that dissociation is not driven near completion (both of these conditions are usually met for blunt-body entry). A large amount of the energy that would have gone into increasing the static temperature behind the bow shock is thus used in exciting vibration energy levels or dissociating the gas molecules. As additional energy is absorbed by the gas molecules entering the shock layer, the conservation laws and the thermophysics of the gas dictate certain changes in the forebody flow. The static temperature, speed of sound, and velocity in the real-gas shock layer are reduced. The static pressure is increased slightly. The density is increased considerably, and the shock-layer thickness is reduced in proportion to this increase.

Use of a substitute gas in simulating the inviscid aerodynamics on blunt and slender bodies at moderate to large angles of attack in these highly compressible real-gas flows without simulating enthalpy was presented in reference 2 for blunt bodies and applied to slender bodies at high angles of attack in references 3 and 4. The contentions therein, references 2, 3, and 4, were as follows: (1) For hypersonic flow conditions, aerodynamic characteristics of blunt bodies are determined primarily by the inviscid flow field which, in turn, is most influenced by the shock density ratio (an indicator of the amount of real-gas effects present) in the blunt, forebody regions where subsonic flows persist and by the local isentropic exponent and local Mach number aft of the forebody in supersonic regions. (2) For ground tests at hypersonic Mach numbers where no dissociation occurs, the density ratio across a shock is determined by the specific-heat ratio of the gas; thus, ground-test data obtained at hypersonic Mach numbers at various values of specific-heat ratio (or shock density ratio) could be used to simulate the trends of equilibrium real-gas effects expected in flight.

Due to dissociation of the gas in the shock layer, shock density ratios as high as 15 and 20 are encountered during planetary entry; however, wind tunnels using air or nitrogen and operating at perfect gas conditions are limited to shock density ratios of less than 6. By using tetrafluoromethane (CF_4) as the test gas in a Mach 6 tunnel (ref. 2), density ratios as high as 12 have been obtained at total temperatures less than 800 K with no dissociation. These high density ratios are possible because of the very low ratio of specific heats of the large CF_4 molecules; this CF_4 tunnel operates virtually as if it had a perfect gas flow with a specific-heat ratio of 1.12.

The high cost of tetrafluoromethane (CF_4, \$8.80 per lb, July 1974) and the need to extend the density-ratio-simulation range above 12 at hypersonic Mach numbers has led to an exploratory experimental and theoretical investigation of the possibilities of using hexafluoroethane (C_2F_6, \$3.00 per lb, July 1974) as an undissociated test gas in a wind tunnel to simulate the aerodynamic characteristics of blunt bodies. The purpose of this investigation is, therefore, to determine whether or not the use of C_2F_6 as a test gas in wind tunnels is a feasible method of obtaining test conditions with large normal-shock density ratios (the necessary condition for blunt-body inviscid similitude).

SYMBOLS

A,B,C,D,E,F	constants in saturation pressure equation (eq. (A15))
a,b,c,d,f	constants in equation for specific heat at zero pressure (eq. (A3))
a_a	speed of sound

c_p	specific heat at constant pressure
c_v	specific heat at constant volume
c'_v	ideal-gas specific heat at constant volume
H	enthalpy
k	thermal conductivity
k*	thermal conductivity at atmospheric pressure
M	Mach number
m	molecular weight
N_{Re}	free-stream Reynolds number (based on base diameter)
p	pressure
R	gas constant (eq. (A1))
r	radius
S	entropy
T	temperature
u	velocity
V	specific volume
Z	compressibility factor, pV/RT
α,β	constants in equation of state (eq. (A1))
γ	ratio of specific heats, c_p/c_v
γ_{eff}	effective value of γ

γ_{ie}	isentropic exponent (eq. (A12))
Δ	shock standoff distance
ϵ	inverse density ratio, ρ_1/ρ_2
μ	viscosity
μ^*	viscosity at atmospheric pressure
ξ	viscosity parameter, $\frac{T_c^{1/6}}{m^{1/2}p_c^{2/3}}$
ρ	density, $1/V$
ρ_R	reduced density, V_c/V
σ	proportionality constant (eq. (A17))
Ω	constant in equation (A18)

Subscripts:

c	critical point
r	reference conditions
s	saturation
0	free-stream stagnation conditions
1	free-stream static conditions
2	static condition behind normal shock
3	stagnation condition behind normal shock

SIMULATION OF REAL-GAS EFFECTS ON BLUNT BODIES

At supersonic and hypersonic speeds, the aerodynamic characteristics, including the lift, drag, moments, and stability, of blunt (high drag, low fineness ratio) configurations are determined almost exclusively by the forebody flow field. Several previous investigations (refs. 5 to 8) have shown, for example, that the drag of such configurations in a constant γ flow (air) is insensitive to Mach number. Other investigations (refs. 2, 7, 8, and 9) have shown that for very high speeds such configurations have aerodynamic characteristics that, although essentially independent of Mach number, are strongly dependent on real-gas effects such as excitation of vibrational energy levels or dissociation. These real-gas effects have been shown to correlate as a function of density ratio across the strong bow shock (ρ_1/ρ_2) for blunt configurations.

The changes in aerodynamic characteristics due to real-gas effects associated with high-speed flight (characterized by large shock density ratios) are primarily the results of changes in surface pressures acting on the forebody. The surface pressures are affected by a change in shock density ratio (real-gas effects) in two ways: first, the level of pressure at the stagnation point is changed, and, second, distribution of surface pressure relative to stagnation-point pressure is changed (for details, see refs. 2 and 10). The investigation of reference 2 was restricted to bodies on which sonic velocities occur at the point of maximum body radius. This is not to say that the density ratio is not a simulation parameter on blunt bodies where the sonic line has moved forward of the point of maximum body radius.

One way to simulate inviscid real-gas effects on blunt bodies is to test in a substitute gas flow which provides the correct value of density ratio without any dissociation. The shock density ratio in the substitute gas is a function of both M_1 and γ. For an ideal gas (ref. 11), the expression for the density ratio across a normal shock is

$$\frac{\rho_2}{\rho_1} = \frac{(\gamma + 1)M_1^2}{(\gamma - 1)M_1^2 + 2} \tag{1}$$

An effective value γ_{eff} can be defined as the ideal or substitute gas value which gives the correct normal-shock density ratio when the free-stream Mach number in equation (1) is used. The distribution of density ratio with shock angle in flight is such that matching the normal-shock density ratio also insures matching of the oblique-shock density ratio for shock angles above 50°. At large hypersonic Mach numbers, the density ratio becomes a function of γ only; however, as γ decreases, the Mach number at which this condition is reached increases.

CHARACTERISTICS OF HEXAFLUOROETHANE

Hexafluoroethane (Freon-116, C_2F_6) is a nonlinear polyatomic molecule. Its 17 vibrational energy modes (ref. 12) display anharmonic oscillator characteristics having 11 fundamental frequencies, 6 of which are twofold degenerate. The acute temperature dependence of the vibrational energy of this molecule reveals itself in the specific heats at constant pressure and volume (c_p and c_v) and their extremely low ratio γ along with the isentropic expansion exponent (γ_{ie}).

Gaseous undissociated hexafluoroethane is colorless, odorless, and nontoxic. Toxic decomposition products may be formed upon thermal or electrical breakdown. However, C_2F_6 is among the most stable of organic compounds (refs. 13 and 14). Reaction with quartz does not occur below about 873 K, and homogeneous decomposition is not appreciable at 1115 K (ref. 13). Some of the physical properties of C_2F_6 (obtained from E. I. du Pont de Nemours & Co.) are:

Molecular weight	138
Boiling point at 1 atm (101.3 kN/m^2), K	194.8
Freezing point, K	172.4
Critical temperature, K	292.7
Critical pressure, atm	29.4
Critical volume, cm^3/mol	225
Critical density, kg/m^3	611
Density, liquid at 200 K, kg/m^3	1587
Density, saturated vapors at boiling point, kg/m^3	9.01
Specific heat, liquid at 200 K, kJ/kg-K	0.971
Estimated specific heat, vapors at 1 atm and 298 K, kJ/kg-K	0.761
Estimated specific-heat ratio at 1 atm and 298 K	1.085
Heat of vaporization at boiling point, kJ/kg	117.04
Vibrational relaxation time at 298 K and 1 atm (ref. 15), sec	2.7×10^{-8}
Thermal conductivity at 298 K and 1 atm, W/m-K	0.017
Prandtl number at 298 K and 1 atm	0.63
Viscosity at 298 K and 1 atm, N-s/m^2	1.4×10^{-5}

PREDICTED AERODYNAMIC SIMULATION IN C_2F_6

In order to duplicate large hypersonic-flight density ratios in a wind tunnel without dissociation, the test gas must have a low ratio of specific heats and a relatively high degree of thermal stability (will not dissociate over the operating temperature range). Also, nonequilibrium and condensation in the test flow are highly undesirable; therefore,

the test gas should have a vibrational relaxation time that is low compared with the time required for the flow to span the shock standoff distance and a vapor pressure that is above the static pressure of the test flow. On the basis of the above criteria, the physical characteristics (see section entitled "Characteristics") indicate that hexafluoroethane may be a promising candidate for high-density-ratio flow simulation.

In order to evaluate the suitability of hexafluoroethane as a test gas for high-density-ratio simulation, a computer code was developed (using the equation presented in the appendix with the shock-crossing equations of ref. 2) to calculate equilibrium conditions for isentropic expansion and flow across normal and oblique shocks in C_2F_6. The structure of this code, along with the shock crossing mechanics, is identical to that given for a CF_4 code in reference 2. Some of the flow variables of interest which were computed from the computer code have been plotted as functions of pertinent parameters for the ranges of stagnation chamber pressure and temperature studied for stream Mach numbers from 3 to 7. A few of the variables of interest are given for CF_4 at the design stagnation condition of a CF_4 wind tunnel for comparative purposes. The stagnation enthalpy H_0 of C_2F_6, which is practically independent of stagnation pressure in the range from 1034 to 1724 N/cm^2, is given as a function of stagnation temperature T_0 in figure 1. Plots of u_1, $\rho_1 u_1^2/2p_0$, T_1/T_0, p_1/p_0, γ_1, γ_2/γ_1, ρ_2/ρ_1, $\rho_1 u_1/\mu_1$, $\rho_2 u_2/\mu_2$, p_3/p_0, and p_3/p_1 against M_1 for C_2F_6 are presented in figures 2 to 12 for T_0 = 478, 588, 700, and 811 K. Specific-heat ratio, the unit Reynolds number, and the Reynolds number behind a normal shock are given for stagnation pressures of 1034, 1378, and 1724 N/cm^2. The other flow variables are independent (within the accuracy of the plots) of stagnation pressure in the range from 1034 to 1724 N/cm^2.

Figure 4 shows the static temperature dropping below the critical at Mach 3.8 for T_0 = 478 K, at Mach 5.2 for T_0 = 588 K, at Mach 6.4 for T_0 = 700 K, and above Mach 7 for T_0 = 811 K. However, the pressure required for condensation (vapor pressure) is much higher than the static pressure (fig. 5) over the Mach number range and stagnation conditions of this study; therefore, condensation does not occur.

The similitude principle adhered to herein is to simulate the inviscid aerodynamics on hypersonic blunt bodies by matching the density ratio across the normal shock. For a given Mach number the normal-shock density ratio is shown to depend only on the γ of the gas media in equation (1). Figure 6 shows that for a temperature of 811 K the γ C_2F_6 remains below 1.10 up to a Mach number of 7, whereas it exceeds 1.20 for CF_4 at these conditions. A comparison of figures 6(a), 6(b), and 6(c) shows that the free-stream γ becomes independent of pressure when the stream Mach number exceeds 3. Calculations indicate that the stream isentropic exponent (γ_{ie}) becomes essentially equal to the specific-heat ratio (γ) once the stream Mach number exceeds 4. The shock specific-heat

ratio γ_2/γ_1 is given in figure 7 as 0.985 at a Mach number of 6 for a total temperature of 811 K. This corresponds (fig. 6) to a free-stream γ of 1.069 and a γ behind the shock of 1.052. Figure 8 shows that for a temperature of 811 K a shock density ratio of 17.6 is obtained at a Mach number of 6 $\left(\gamma_{eff} = 1.059\right)$. In CF_4 a density ratio of 12 is obtained at these same test conditions $\left(\gamma_{eff} = 1.12\right)$. Scanning the stagnation condition of figure 8 for a Mach number range of 5 to 7 gives a density-ratio range of from 13 to 20.

Inclusion of viscous regions in the aerodynamic similitude of blunt-body flows (incompressible flow) requires matching local Reynolds number. The unit Reynolds numbers for the previously stated range of test conditions are given in figure 9. They are much lower than that for air at the same stagnation conditions. The Reynolds number range for a C_2F_6 Mach 6 tunnel based on a model length of 0.3 m would be 1.0×10^5 to 4.0×10^6.

The Reynolds number behind a normal shock in C_2F_6 is given as a function of Mach number in figure 10. The Reynolds number behind the normal shock in C_2F_6 at $M_1 = 6$ is lower $\left(5 \times 10^6/\text{m}$ versus $4 \times 10^5/\text{m}\right)$ than that in CF_4 at $M_1 = 6$ for the same stagnation conditions $\left(T_0 = 478\ \text{K};\ p_0 = 1724\ \text{N/cm}^2\right)$, but of the same order of a Mach 6 air wind tunnel $(5 \times 10^5/\text{m})$ at normal operating conditions. The large Reynolds number behind the normal shock in CF_4 and C_2F_6 is due primarily to the large density behind the shock. In flight, where real-gas effects are prominent, large Reynolds numbers also occur behind shocks because of the large density. Noting that in any simulation it is the local conditions which should be simulated and not necessarily the free-stream ones, C_2F_6 and other high-density-ratio (low γ) substitute gases may come nearer to simulating the local Reynolds number on a vehicle at flight conditions where real-gas effects are prominent than high Reynolds number air or helium tunnels (ideal gas-high γ). This is especially true if the local Reynolds number and local Mach number simulation capability is examined behind 20° to 50° oblique shocks when the normal-shock-density-ratio conditions are matched, since the low γ gases also give higher Mach numbers behind oblique shocks than do the high γ gases.

The shock density ratio and Reynolds number simulation capability of CF_4 and C_2F_6 (assuming 10.15-cm-diameter model and a realistic pressure range) is shown in figure 13 and that of several facilities at the Langley Research Center, which are thought to be typical of most facility capabilities, is shown in figure 14. Also shown in both figures are two entry trajectories typical of very blunt high-drag vehicles. Both these trajectories are based on the assumption of chemical equilibrium in the shock layer. The Earth entry trajectory is for an angle of 90°, an entry velocity of 5600 m/sec, a ballistic coefficient of 146 kg/m^2, and a diameter of 0.67 m. The Mars trajectory is for an assumed atmosphere

of 2000 N/m^2 (model 2, ref. 16), an entry angle of 90°, an entry velocity of 8700 m/sec, a ballistic coefficient of 23.5 kg/m^2, and a diameter of 5 m. The "knee" of the trajectories corresponds roughly to conditions of peak heating and peak dynamic pressure. The Reynolds number behind the shock would be a better simulation parameter than that of the free stream to use in figures 13 and 14; this would show both CF_4 and C_2F_6 in an even more favorable light concerning the simulation of the two trajectories. Since the aerodynamics of blunt bodies depends essentially only on the shock density ratio, the aerodynamics of a blunt Mars entry vehicle could be simulated over almost the entire Mars entry trajectory (fig. 13) in C_2F_6. An examination of figures 13 and 14 shows that with C_2F_6 the ability to simulate shock density ratios which occur with high-speed atmospheric entry is increased from 14 to 20.

EXPERIMENTAL TEST AND RESULTS

Apparatus

Exploratory experimental tests were conducted in the Langley pilot CF_4 Mach 6 tunnel (ref. 2) to evaluate the suitability of C_2F_6 as a test gas. The tunnel is an intermittent type that is supplied by two large bag-type accumulators. These accumulators maintain a constant tunnel stagnation pressure for times as long as 3 min. The gas passes from the accumulators through a lead-bath heat exchanger (stainless steel tubes immersed in a bath of molten lead) into the stagnation chamber and through the tunnel nozzle. The tunnel's contoured axisymmetric nozzle was designed for a CF_4 flow at Mach 6 for stagnation conditions of 811 K and 1724 N/cm^2. The nozzle is 67 cm long with a 16.4-cm-diameter test section. The expansion (area) ratio of this nozzle is 2569. The tunnel exhausted into a 1200-m^3 vacuum sphere which could be pumped to pressures as low as 25 N/m^2. No attempts were made to reclaim the C_2F_6, although it should be possible to do so easily since it is a heavy gas with a relatively high critical temperature (292.7 K) and a relatively low critical pressure (29.4 atm). To keep the gas above the critical temperature during pumping from the storage bottles to the accumulators (to avoid consensation at the high pressures), the storage bottles and transport lines were wrapped with strip heaters and heated to 316 K. This facility description and operational procedure verifies the practicality of using C_2F_6 as a test gas in a hypersonic wind tunnel.

Experimental Tests

Tunnel survey.- A pitot rake with six orifices spanning 11.3 cm of the 16.4-cm-diameter test section was used to survey the C_2F_6 test stream for three stagnation conditions. These conditons were:

Survey test	p_0, N/cm^2	T_0, K
1	948	520
2	1265	581
3	1565	603

The results of the pitot surveys are shown in figure 15. The uniformity of the Mach number distributions are acceptable over the 10.3-cm span, and the level $M_1 \approx 5.4$ is consistent with that predicted from the real-gas (C_2F_6) computer code for the area ratio of the nozzle. The tunnel-wall static pressure in the test section was measured during each of these tests. The Mach number corresponding to the static pressure is also shown in figure 15 and is reasonably consistent with that corresponding to the total pressure measurements.

Hemisphere tests.- Tests were conducted on a 1-in.-diameter hemisphere with a pressure orifice at its stagnation point at essentially the same three test conditions as that of the pitot surveys. Shadowgraphs of the bow shock (fig. 16) along with the pressure at the stagnation point of the model were obtained. Normal-shock density ratios in the test section were determined from the shock standoff distance measured on the hemisphere (fig. 16) by using the following relation (ref. 2):

$$\frac{\rho_2}{\rho_1} = \frac{0.76}{\Delta/r}$$

The normal shock density ratio obtained from the shock standoff distance along with the Mach number (M_{calc}) calculated from the stagnation point pressures and the corresponding calculated density ratios $(\rho_2/\rho_1)_{calc}$ for each of these tests are:

Survey test	p_0, N/cm^2	T_0, K	$(\rho_2/\rho_1)_{exp}$	M_{calc}	$1)_{calc}$
4	903	505	14	5.40	14.3
5	1250	580	14	5.40	14.3
6	1500	589	15	5.35	15.1

The Mach numbers are consistent with those obtained with the survey rake and the calculated density ratios (fig. 15). The density ratios obtained fron he shock standoff distance (eq. (2)) are in reasonable agreement with those obtained from isentropic expansion normal-shock calculations (fig. 8).

The influence of the density ratio on the shock shape of a hemisphere is illustrated in figure 17 where sketches of shock shapes in air, CF_4, and C_2F_6 are given at density

ratios of 5.6, 12, and 16, respectively. The shock wave for the higher density ratio (C_2F_6) is much closer to the body. Furthermore, since it lies closer to the body, the expansion waves from the body and the expansion fan from the corner bends it more sharply and thus the shock angle reaches its limiting value more rapidly than for the lower density ratio shocks. This comparison of the shock shapes indicates that even though the limiting shock angle is 7.2° for air at Mach 8, 9.4 for CF_4 at Mach 6.1, and 10.7° for C_2F_6 at Mach 5.4, a downstream distance of many diameters would be required before the shocks cross.

CONCLUDING REMARKS

An experimental and theoretical investigation of the use of hexafluoroethane $(\text{Freon-116, } C_2F_6)$ as a test gas in a wind tunnel to simulate the inviscid aerodynamic characteristics of blunt bodies in high-speed flight where dissociation takes place in the shock layer indicates the following:

1. The use of C_2F_6 as a test gas in hypersonic wind tunnels is shown to be a practical and relatively inexpensive method of obtaining low specific-heat-ratio (γ) flows with large normal-shock density ratios without dissociation.

2. Calculations indicate that a shock-density-ratio range from 13 to 20 could be achieved with C_2F_6 for free-stream Mach numbers from 5 to 7 with stagnation temperatures below 811 K.

3. Tests made in a small pilot C_2F_6 tunnel confirmed real-gas calculations for test conditions in C_2F_6. Values of normal-shock density ratio as high as 15 were obtained in the pilot C_2F_6 tunnel at a stagnation pressure of 1500 N/cm^2, a stagnation temperature of 589 K, and a free-stream Mach number of 5.35.

4. Since the aerodynamics of blunt bodies depends essentially only on the shock density ratio, the aerodynamics of a blunt Mars entry vehicle could be simulated over almost the entire entry trajectory in C_2F_6.

Langley Research Center,
National Aeronautics and Space Administration,
Hampton, Va., July 5, 1974.

APPENDIX

THERMODYNAMIC AND TRANSPORT EQUATIONS OF GASEOUS HEXAFLUOROETHANE

The thermodynamic property equations of hexafluoroethane (C_2F_6) are derived from the equation of state and the expression for the specific heat at zero pressure. These properties are essential in predicting isentropic flows, flows across normal and oblique shocks, and the inviscid flow fields over vehicles. The transport properties are essential when viscous phenomena such as boundary layers on a nozzle or vehicular walls are being considered.

The equation of state of hexafluoroethane was obtained from E. I. du Pont de Nemours & Co. and is

$$p = \frac{RT}{V - \beta} - \frac{\alpha T^{-1/2}}{V(V + \beta)} \tag{A1}$$

where p is given in N/m^2, V in m^3/kg, and T in K and where

$$R = 6.024225 \times 10 \text{ J/kg-K}$$

$$\beta = 5.133877 \times 10^{-4} \text{ m}^3/\text{kg}$$

$$\alpha = 7.657512 \times 10^{-2} \text{ J-m}^3\text{-K}^{1/2}/\text{kg}^2$$

The specific heat at constant volume is

$$c_V = c'_V + \int_{\infty}^{V} T\left(\frac{\partial 2p}{\partial T^2}\right)_V dV \tag{A2}$$

and c'_V is the specific heat at zero pressure. A third-degree expression in temperature for c'_V (obtained from E. I. du Pont de Nemours & Co.) is:

$$c'_V = a + bT + cT^2 + dT^3 + \frac{f}{T^2} \tag{A3}$$

where c_v' is in J/kg-K and where

$a = 9.952795 \times 10$ J/kg-K

$b = 2.608545$ J/kg-K^2

$c = -1.926454 \times 10^{-3}$ J/kg-K^3

$d = 1.857347 \times 10^{-7}$ J/kg-K^4

$f = -3.473992 \times 10^5$ J-K/kg

Evaluating the integral term of equation (A2) with the equation of state, equation (A1), gives

$$c_v = c_v' + \frac{3\alpha T^{-3/2}}{4\beta} \ln\left(\frac{V + \beta}{V}\right) \tag{A4}$$

The entropy S expressed as a function of T and V is

$$S - S_r = \int_{T_r}^{T} \frac{c_v}{T}\, dT + \int_{V_r}^{V} \left(\frac{\partial p}{\partial T}\right)_V dV \tag{A5}$$

where the subscript r represents reference conditions taken herein as

$S_r = 443.504$ J/kg-K

$T_r = 172.222$ K

$p_r = 2.468323 \times 10^4$ N/m^2

$V_r = 0.41489$ m^3/kg

From the integration of equation (A5) the expression for entropy becomes

$$S - S_r = a \ln\left(\frac{T}{T_r}\right) + b\left(T - T_r\right) + \frac{c}{2}\left(T^2 - T_r^2\right) + \frac{d}{3}\left(T^3 - T_r^3\right) - \frac{f}{2}\left(\frac{1}{T^2} - \frac{1}{T_r^2}\right)$$

$$+ R \ln\left(\frac{V - \beta}{V_r - \beta}\right) - \frac{\alpha}{2\beta} T_r^{-3/2} \ln\left(\frac{V_r}{V_r + \beta}\right) + \frac{\alpha T^{-3/2}}{2\beta} \ln\left(\frac{V}{V + \beta}\right) \tag{A6}$$

The enthalpy H expressed as a function of T and V is

$$H - H_r = \int_{T_r}^{T} \left[c_v + V\left(\frac{\partial p}{\partial T}\right)_V \right] dT + \int_{V_r}^{V} \left[V\left(\frac{\partial p}{\partial T}\right)_T + T\left(\frac{\partial p}{\partial T}\right)_V \right] dV \tag{A7}$$

and becomes in integrated form

$$\begin{aligned} H - H_r = {} & a\left(T - T_r\right) + \frac{b}{2}\left(T^2 - T_r{}^2\right) + \frac{c}{3}\left(T^3 - T_r{}^3\right) + \frac{d}{4}\left(T^4 - T_r{}^4\right) - f\left(\frac{1}{T} - \frac{1}{T_r}\right) \\ & - \frac{3}{2}\frac{\alpha}{\beta}\left(T^{-1/2} - T_r{}^{-1/2}\right) + \frac{RV_r}{V_r - \beta}\left(T - T_r\right) - \frac{\alpha}{V_r + \beta}\left(T^{-1/2} - T_r{}^{-1/2}\right) \\ & - \beta RT\left(\frac{1}{V - \beta} - \frac{1}{V_r - \beta}\right) - \alpha T^{-1/2}\left(\frac{1}{V + \beta} - \frac{1}{V_r + \beta}\right) \\ & - \frac{3\alpha T^{-1/2}}{2\beta}\left[\ln\left(\frac{V + \beta}{V}\right) - \ln\left(\frac{V_r + \beta}{V_r}\right)\right] \end{aligned} \tag{A8}$$

where $H_r = 68152.7$ J/kg.

Other variables of interest are:

Specific heat at constant pressure

$$c_p = c_v - T\frac{\left[\left(\frac{\partial p}{\partial T}\right)_V\right]^2}{\left(\frac{\partial p}{\partial V}\right)_T} \tag{A9}$$

Specific-heat ratio

$$\gamma = \frac{c_p}{c_v} = 1 - T\frac{\left[\left(\frac{\partial p}{\partial T}\right)_V\right]^2}{c_v\left(\frac{\partial p}{\partial V}\right)_T} \tag{A10}$$

Speed of sound

$$a_a = \left(\frac{\partial p}{\partial \rho}\right)_S^{1/2} = \left[-\gamma V^2 \left(\frac{\partial p}{\partial V}\right)_T\right]^{1/2} = \left\{\frac{V^2 T}{c_v}\left[\left(\frac{\partial p}{\partial T}\right)_V\right]^2 - V^2\left(\frac{\partial p}{\partial V}\right)_T\right\}^{1/2} \tag{A11}$$

Isentropic exponent

$$\gamma_{ie} = \left(\frac{d \ln p}{d \ln \rho}\right)_S = \frac{\rho}{p}\left(\frac{dp}{d\rho}\right)_S = -\frac{\gamma V\left(\frac{\partial p}{\partial V}\right)_T}{p} = \frac{a_a{}^2}{pV} \tag{A12}$$

where the partial derivatives in equations (A9) to (A12) are

$$\left(\frac{\partial p}{\partial T}\right)_V = \frac{R}{V - \beta} + \frac{\alpha T^{-3/2}}{2V(V + \beta)} \tag{A13}$$

$$\left(\frac{\partial p}{\partial V}\right)_T = -\frac{RT}{(V - \beta)^2} + \frac{\alpha T^{-1/2}(2V + \beta)}{V^2(V + \beta)^2} \tag{A14}$$

These equations are limited to temperatures above the saturated vapor line. The saturation pressure in N/m^2 as a function of temperature in kelvins (obtained from E. I. du Pont de Nemours & Co.) is

$$\log p_S = A + \frac{B}{T} + C \log T + DT + \frac{E(F - T)}{T}\left[\log(F - T) + 0.25527\right] + 0.52553 \tag{A15}$$

where

$$A = 0.3762282521 \times 10^2$$

$$B = -1.031833 \times 10^3$$

$$C = -0.1297816132 \times 10^2$$

$D = 0.01321347$

$E = -0.537560386$

$F = 0.297317 \times 10^3$

This equation is only applicable below the critical temperature $(T_c = 292.7\ K)$. Also, equations (A1) to (A14) are limited to temperatures below those at which dissociation occurs ($T < 1115$ K).

Transport Properties of Gaseous C_2F_6

Viscosity.- An expression for the vapor viscosity of C_2F_6 at 1 atm of pressure was obtained from E. I. du Pont de Nemours & Co; the expression is

$$\mu^* = \left(12.778\sqrt{T} - 78.8\right) \times 10^{-7} \tag{A16}$$

where μ^* is in $N\text{-}s/m^2$ and T is in K. This equation has experimental data to support its validity over a temperature interval from 230 K to 420 K. The viscosity of C_2F_6 at a pressure of 1 atm determined from equation (A16) is plotted over a temperature interval of 150 K to 800 K in figure 18. Even though the curve fit was only made for a temperature interval of 230 K to 420 K, equation (A16) behaves well over the extended range. To obtain the viscosity of C_2F_6 at pressures other than 1 atm, the residual viscosity is expressed as a function of the density, molecular weight, and critical constants of the substance (ref. 17) through a dimensional analysis treatment (ref. 15) resulting in the following expression:

$$(\mu - \mu^*)\xi = \frac{\sigma}{R^{1/6}}\, Z_c{}^i \rho_R{}^j \tag{A17}$$

Experimental high-pressure viscosities for the gaseous and liquid phases available in the literature for 14 polar substances including five Freons $\left(CCl_3F,\ CCl_2F_2,\ CHCl_2F,\ CHClF_2,\right.$ and $\left.C_2Cl_3F_3\right)$ were used (ref. 18) in conjunction with pressure-volume-temperature data to establish the constant σ and the exponents i and j of equation (A17). Plots of $(\mu - \mu^*)\xi$ against ρ_R (ref. 13) were found to be essentially the same for all 14 substances; therefore, it was concluded that the exponent i of Z_c in equation (A17) was zero.

The analytical representation of the residual viscosity correlation for the 14 polar substances (ref. 18) which should apply to C_2F_6 as well are:

$$(\mu - \mu^*)\xi = 16.56 \times 10^{-8}\rho_R^{1.111} \qquad \left(\rho_R \leqq 0.10\right) \qquad \text{(A18a)}$$

$$(\mu - \mu^*)\xi = 0.607 \times 10^{-8}\left(9.045\rho_R + 0.63\right)^{1.739} \qquad \left(0.10 < \rho_R \leqq 0.90\right) \qquad \text{(A18b)}$$

$$-\log\left[(\mu - \mu^*)\xi\right] = 10^{0.6439 - 0.1005\rho_R - \Omega} + 3 \qquad \left(0.9 < \rho_R < 2.6\right) \qquad \text{(A18c)}$$

where $\Omega = 0$ for $0.9 < \rho_R < 2.2$, $\Omega = 4.75 \times 10^{-4}\left(\rho_R^3 - 10.65\right)^2$ for $2.2 < \rho_R < 2.6$, and $\xi = \dfrac{T^{1/6}}{M^{1/2}p_c^{2/3}} = 0.023735$ for C_2F_6 and where μ is in N-s/m^2.

Thermal conductivity.- An estimate for the thermal conductivity of C_2F_6 gas at a pressure of 1 atm was obtained from E. I. du Pont de Nemours & Co. as:

$$k^* = (9.591 \times 10^{-5})T - 0.01163 \qquad \text{(A19)}$$

where k^* is in W/m-K. The estimate was made over a temperature range from 230 K to 420 K. The thermal conductivity at 1 atm of pressure is plotted over a temperature range of 100 K to 800 K in figure 19.

The thermal conductivity relationship is extended to pressure other than 1 atm in the same manner as was the viscosity. Residual thermal conductivities $k - k^*$ for CF_4 were obtained from experimental data and correlated with the corresponding reduced densities (ref. 19) to produce the following expression:

$$k - k^* = 7.18 \times 10^{-3}\left[\exp\left(\rho_R\right) - 1\right] \qquad \text{(A20)}$$

where $k - k^*$ is in W/m-K. Equation (A20) represents the thermal conductivity of CF_4 in the dense gaseous region and should also be fairly representative of the thermal conductivity of C_2F_6.

REFERENCES

1. Nagel, A. L.; and Thomas, A. C.: Analysis of the Correlation of Wind Tunnel and Ground Test Data to Flight Test Results. AIAA Paper No. 65-208, Feb. 1965.

2. Jones, Robert A.; and Hunt, James L. (With appendix A by James L. Hunt, Kathryn A. Smith, and Robert B. Reynolds, and appendix B by James L. Hunt and Lillian R. Boney): Use of Tetrafluoromethane To Simulate Real-Gas Effects on the Hypersonic Aerodynamics of Blunt Vehicles. NASA TR R-312, 1969.

3. Hunt, James L.; and Creel, Theodore R., Jr.: Shock Interference Heating and Density-Ratio Effects. Part II – Hypersonic Density-Ratio Effects. NASA Space Shuttle Technology Conference, Vol. I, NASA TM X-2272, 1971, pp. 217-243.

4. Hunt, James L.; and Jones, Robert A.: Heating and Flow-Field Studies on a Straight-Wing Hypersonic Reentry Vehicle at Angles of Attack From 20° to 80° With Simulation of Real-Gas Trends. NASA TN D-7108, 1973.

5. Walker, Billy; and Weaver, Robert W.: Static Aerodynamic Characteristics of Blunted Cones in the Mach-Number Range From 2.2 to 9.5. Tech. Rep. 32-1213 (Contract No. NAS 7-100), Jet Propulsion Lab., California Inst. Technol., Dec. 1, 1967.

6. Campbell, James F.: Supersonic Aerodynamic Characteristics and Shock Standoff Distances for Large-Angle Cones With and Without Cylindrical Afterbodies. NASA TN D-5334, 1969.

7. Anon.: Comparative Studies of Conceptual Design and Qualification Procedures for Mars Probe/Lander. Volume V: Subsystem and Technical Analysis – Book 2: Aeromechanics and Thermal Control. AVSSD-0006-66-RR (Contract NAS 1-5224), AVCO Corp., May 11, 1966. (Available as NASA CR-66136.)

8. Krumins, M. V.: Drag and Stability of Various Mars Entry Configurations. Propulsion Re-Entry Physics, P. Contensov, G. N. Duboshin, and W. F. Hilton, eds., Pergamon Press, Inc., 1970, pp. 337-360.

9. Allison, Dennis O.; and Bobbitt, Percy J.: Real-Gas Effects on the Drag and Trajectories of a Nonlifting 140° Conical Aeroshell During Mars Entry. NASA TN D-6240, 1971.

10. Jones, Robert A.; and Hunt, James L.: Measured Pressure Distributions on Large-Angle Cones in Hypersonic Flows of Tetrafluoromethane, Air and Helium. NASA TN D-7429, 1973.

11. Ames Research Staff: Equations, Tables, and Charts for Compressible Flow. NACA Rep. 1135, 1953. (Supersedes NACA TN 1428.)

12. Anon.: JANAF Thermochemical Tables. Second ed. NSRDS-NBS 37, U.S. Dep. Com., June 1971.

13. White, Locke, Jr.; and Rice, O. K.: The Thermal Reaction of Hexafluoroethane With Quartz. J. Amer. Chem. Soc., vol. 69, no. 1, Jan. 1947, pp. 267-270.

14. Steunenberg, Robert K.; and Cady, George H.: Pyrolysis of Fluorocarbons. J. Amer. Chem. Soc., vol. 74, no. 16, Aug. 20, 1952, pp. 4165-4168.

15. Lambert, J. D.; and Salter, R.: Vibrational Relaxation in Gases. Proc. Roy. Soc. (London), ser. A, vol. 253, no. 1273, Nov. 24, 1959, pp. 277-288.

16. Levin, George M; Evans, Dallas E.; and Stevens, Victor, eds.: NASA Engineering Models of the Mars Atmosphere for Entry Vehicle Design. NASA TN D-2525, 1964.

17. Jossi, John A.; Stiel, Leonard I.; and Thodos, George: The Viscosity of Pure Substances in the Dense Gaseous and the Liquid Phases. AIChE J., vol. 8, 1962, pp. 59-63.

18. Stiel, Leonard I.; and Thodos, George: The Viscosity of Polar Substances in the Dense Gaseous and Liquid Regions. AIChE J., vol. 10, no. 2, 1964, pp. 275-277.

19. Oshen, Steven; Rosenbaum, B. M.; and Thodos, George: Thermal Conductivity of Carbon Tetrafluoride in the Dense Gaseous Region. J. Chem. Phys., vol. 46, no. 8, Apr. 15, 1967, pp. 2939-2944.

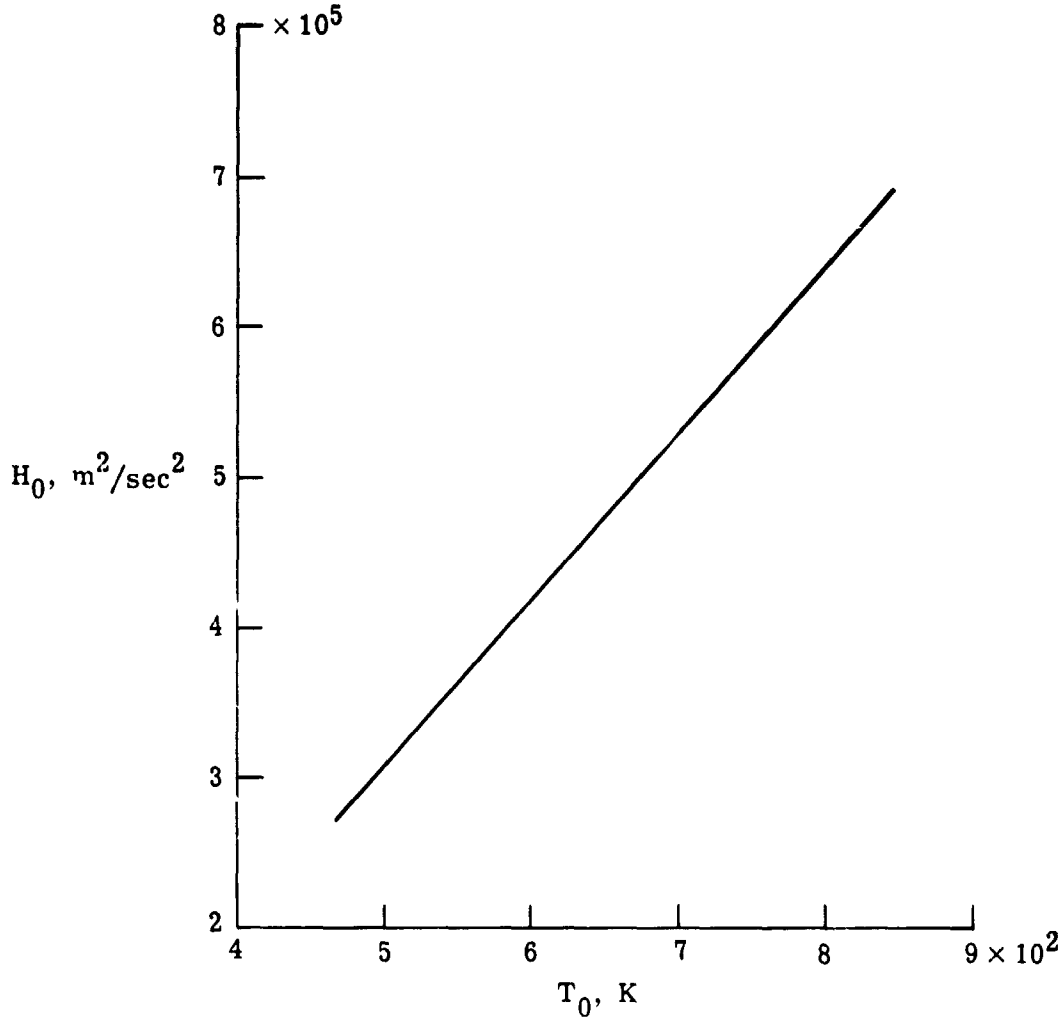

Figure 1.- Total enthalpy of C_2F_6. (Independent of stagnation pressure from 1031 to 1724 N/cm^2.)

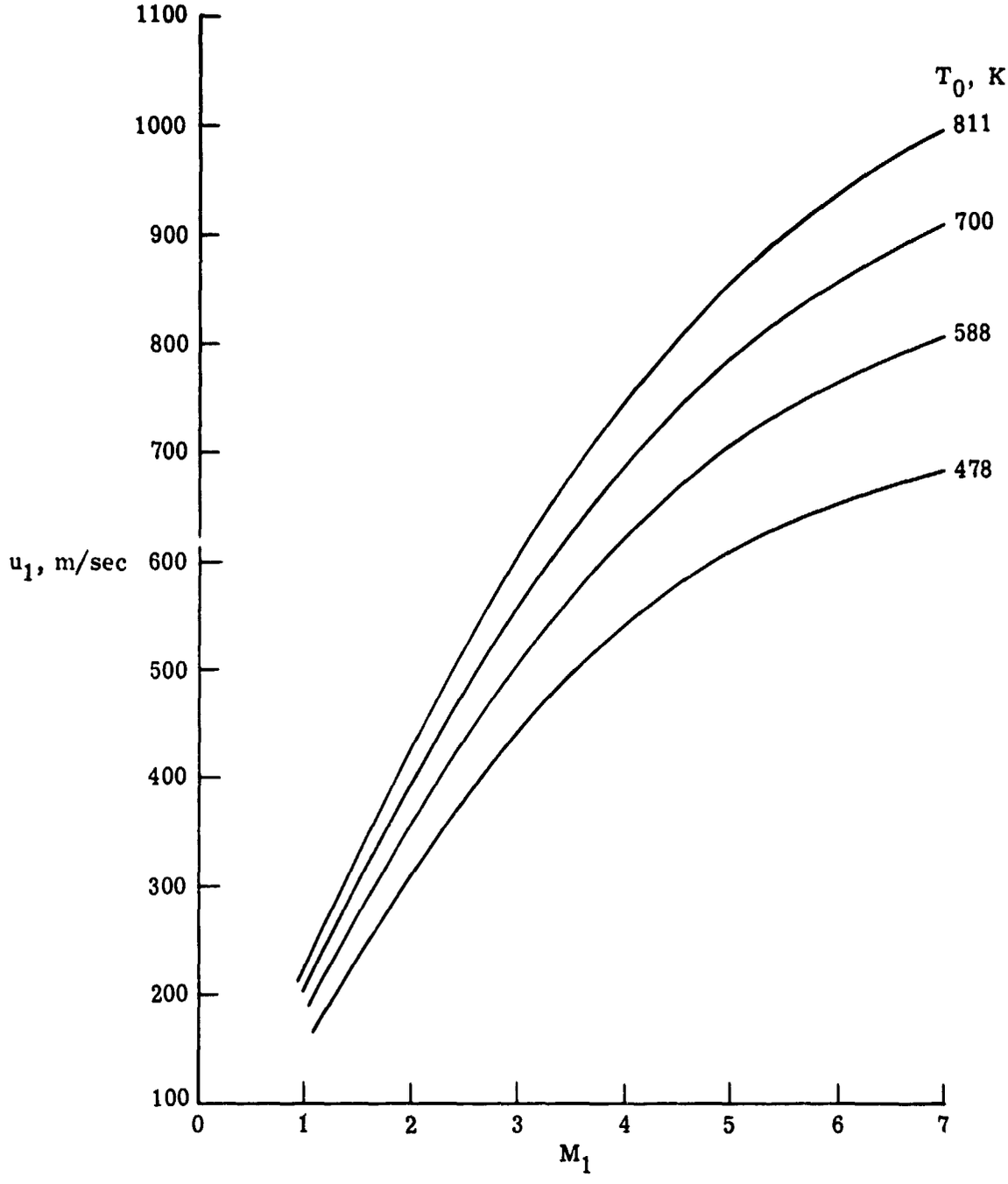

Figure 2.- Variation of free-stream velocity with Mach number for C_2F_6. (Independent of stagnation pressure from 1034 to 1724 N/cm^2.)

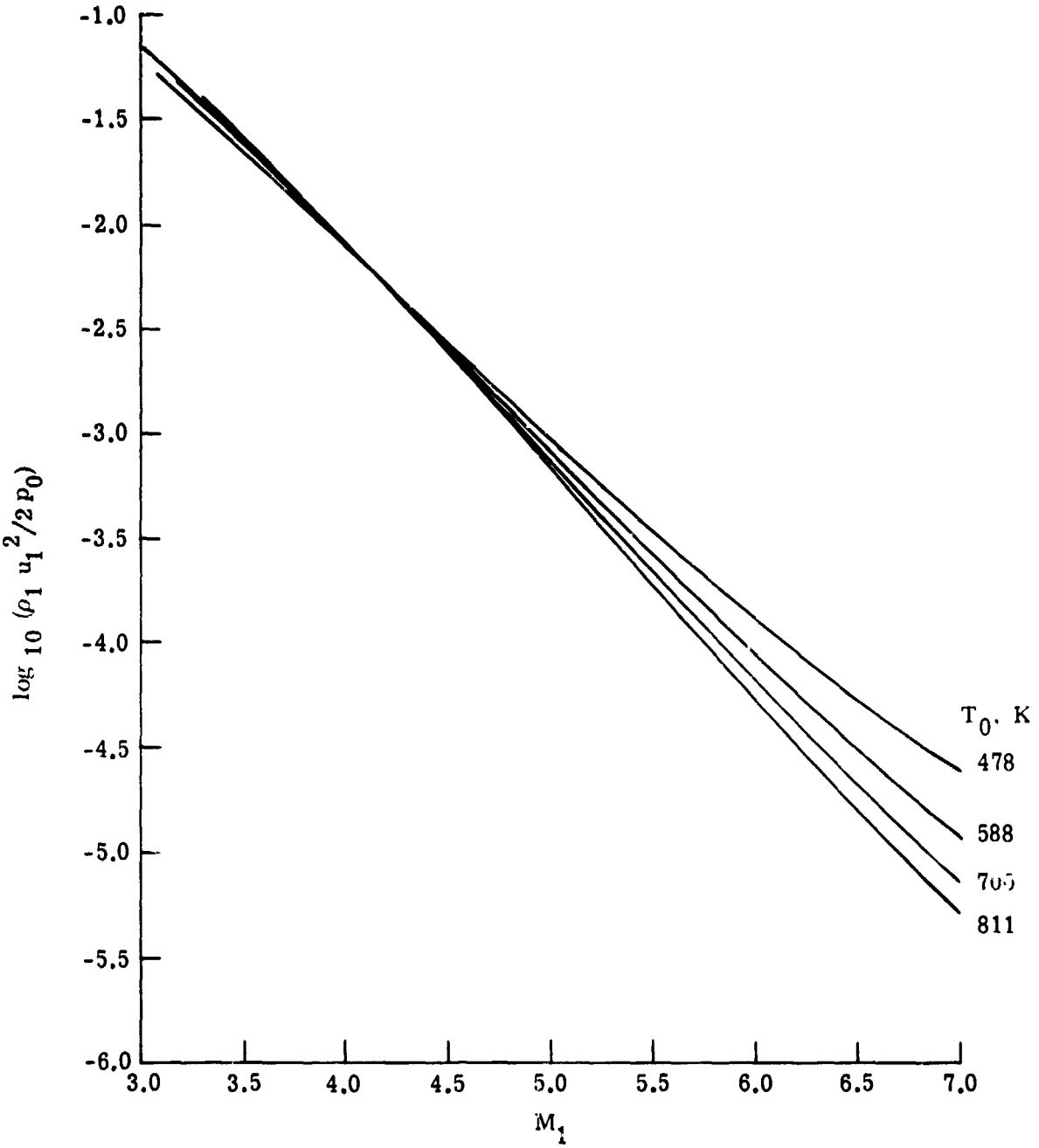

Figure 3.- Variation of ratio of free-stream dynamic pressure to stagnation pressure with Mach number for C_2F_6. (Independent of stagnation pressure from 1034 to 1724 N/cm^2.)

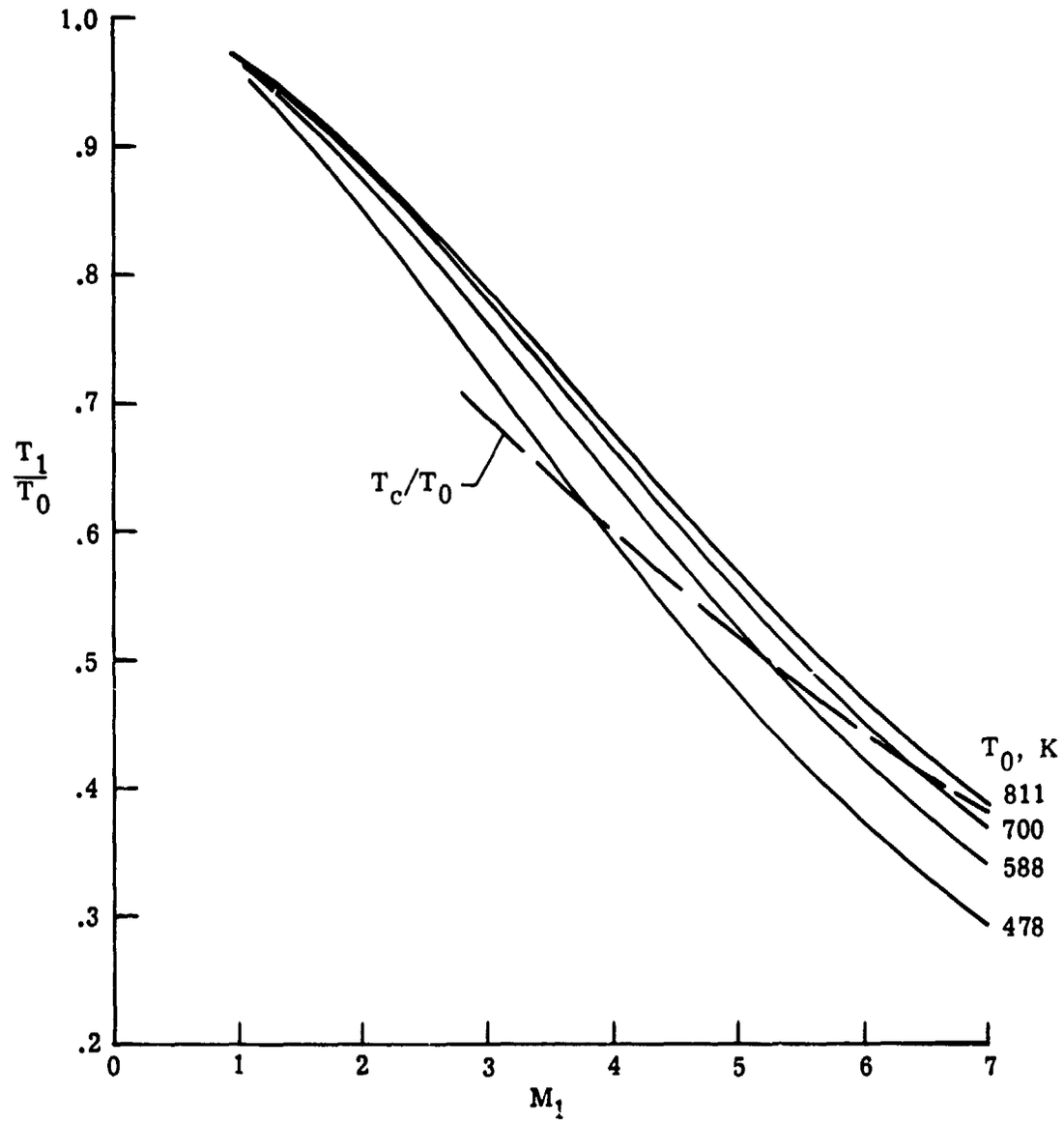

Figure 4.- Variation of ratio of free-stream static temperature to stagnation temperature with Mach number for C_2F_6. (Independent of stagnation pressure from 1034 to 1724 N/cm^2.)

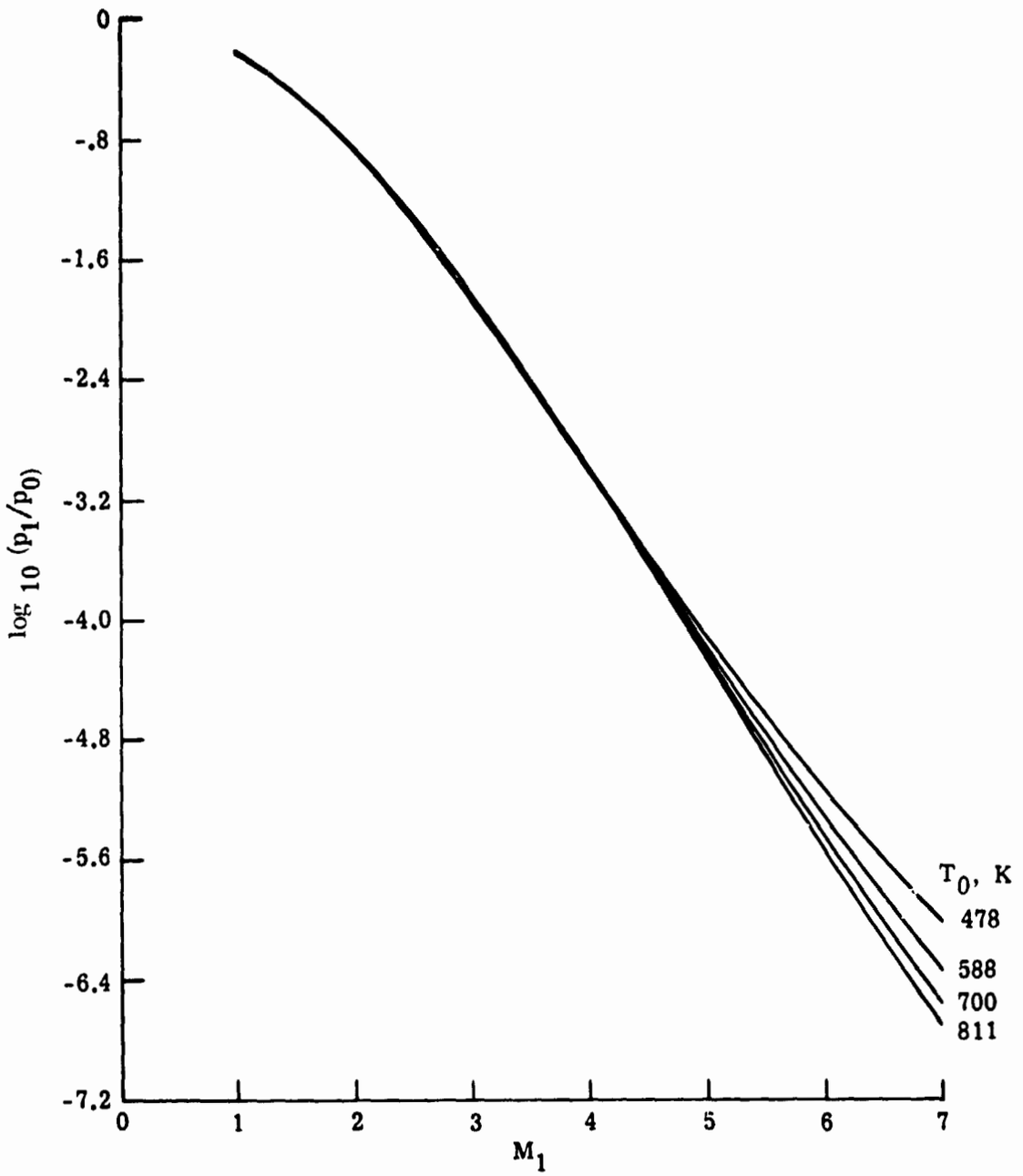

Figure 5.- Variation of ratio of free-stream static pressure to stagnation pressure with Mach number for C_2F_6. (Independent of stagnation pressure from 1034 to 1724 N/cm^2.)

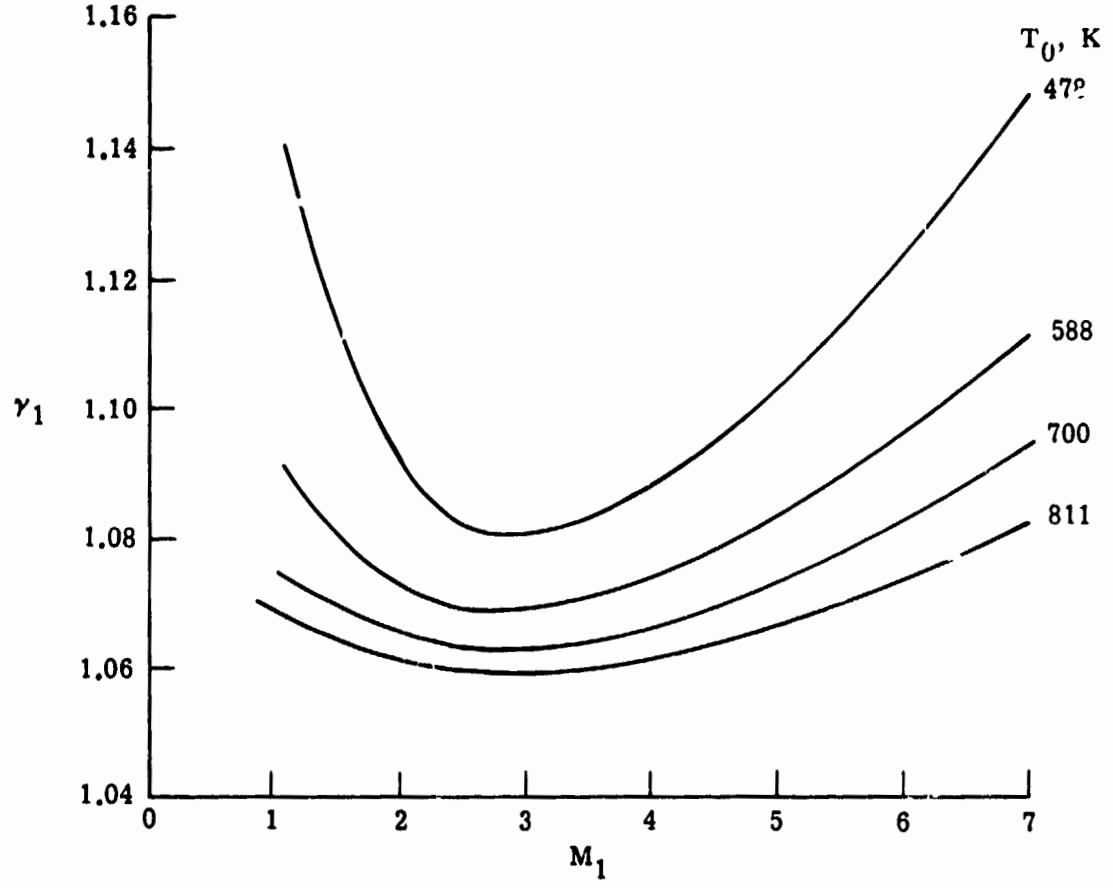

(a) $p_0 = 1034$ N/cm^2.

Figure 6.- Variation of free-stream specific-heat ratio with Mach number for C_2F_6.

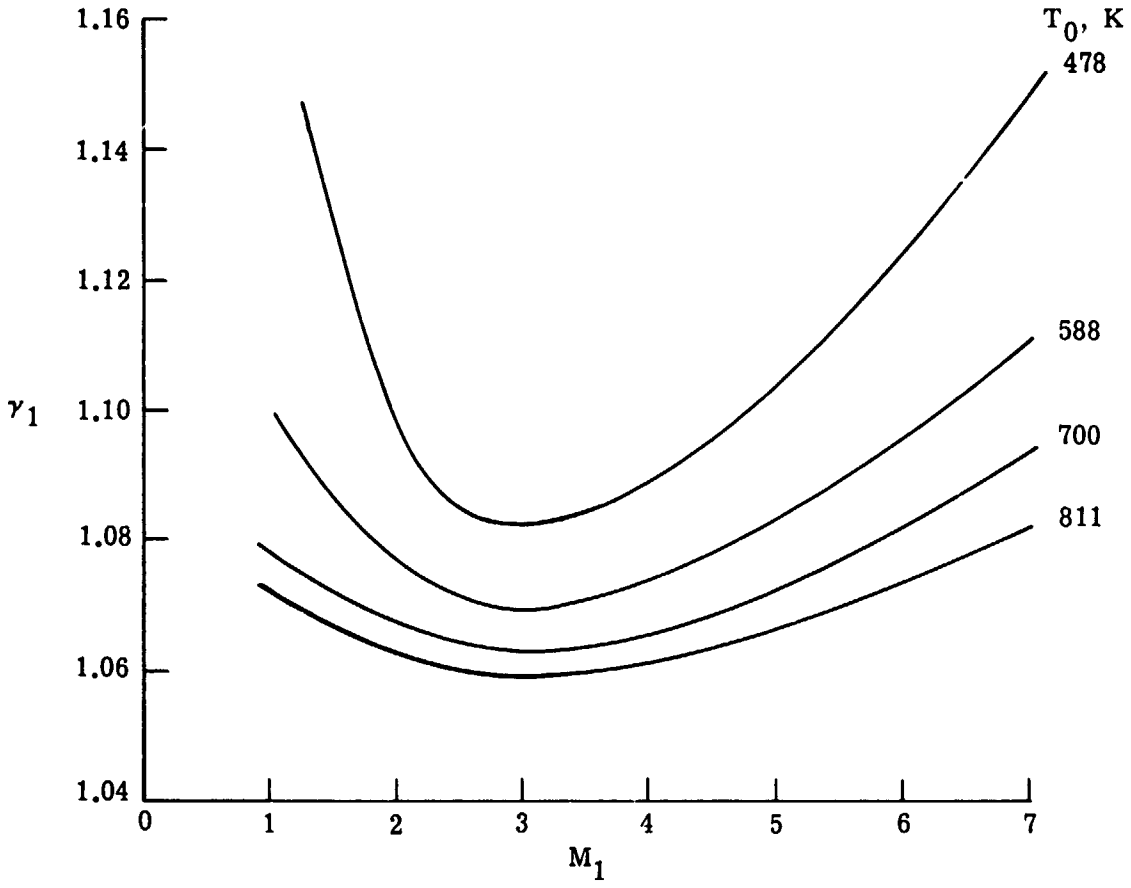

(b) $p_0 = 1378\ N/cm^2$.

Figure 6.- Continued.

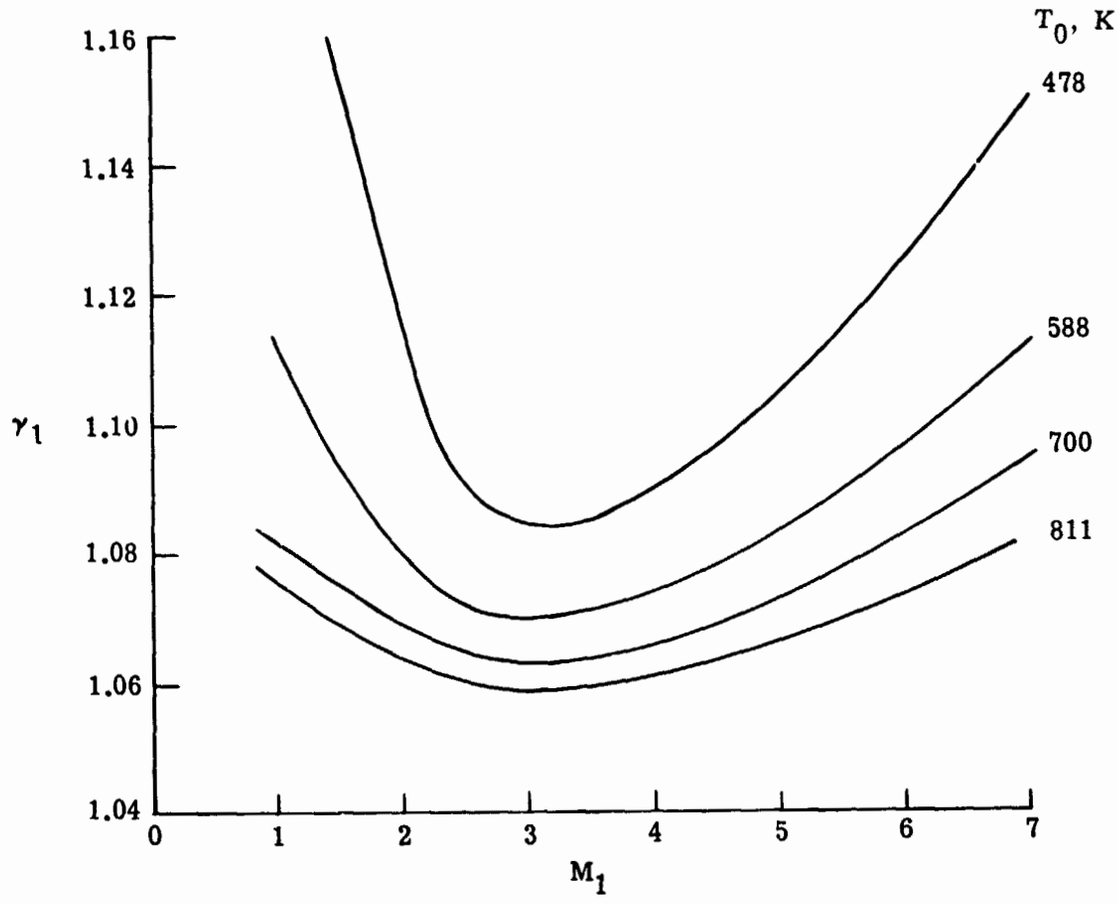

(c) $p_0 = 1724$ N/cm^2.

Figure 6.- Concluded.

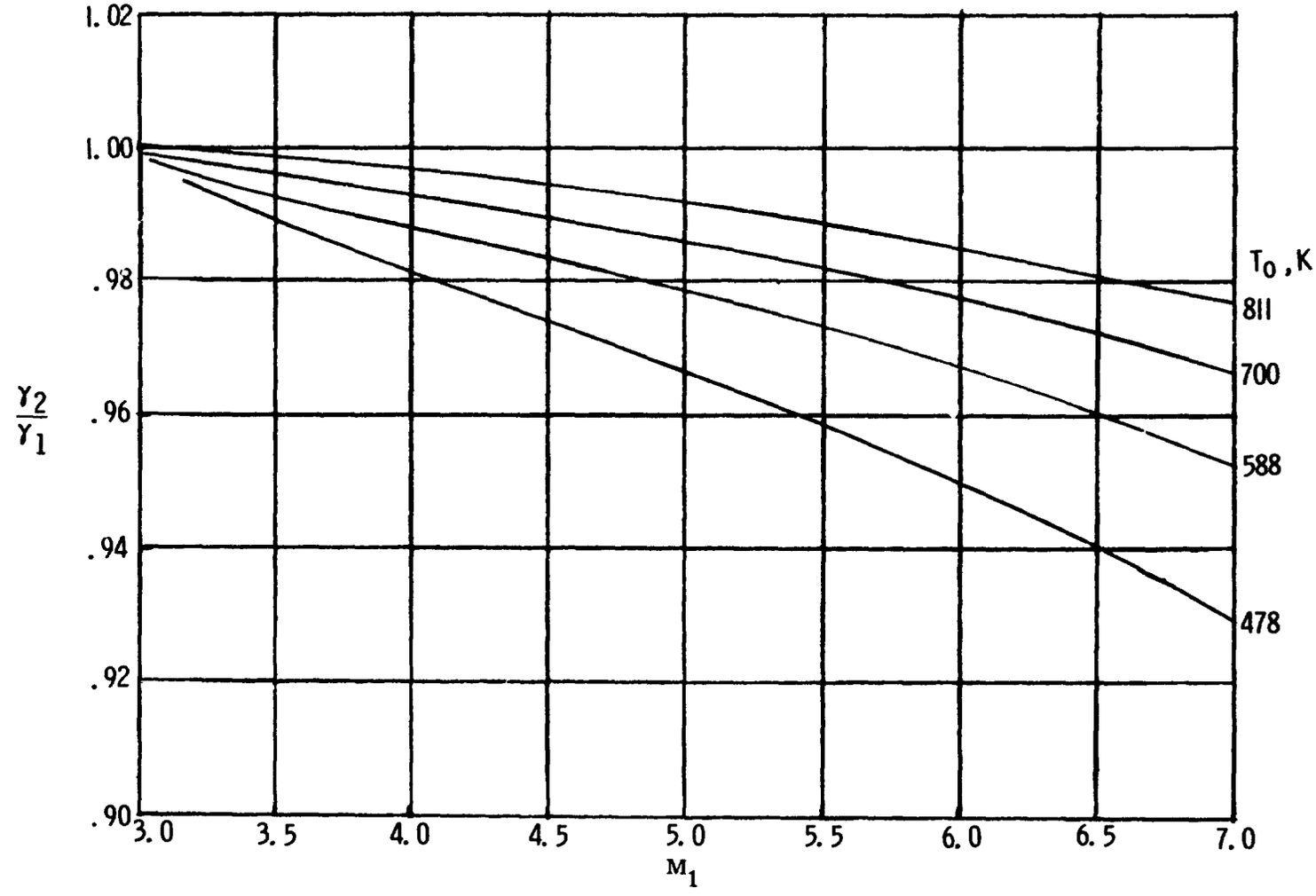

Figure 7.- Variation of γ_2/γ_1 with Mach number for C_2F_6. (Independent of stagnation pressure from 1034 to 1724 N/cm^2.)

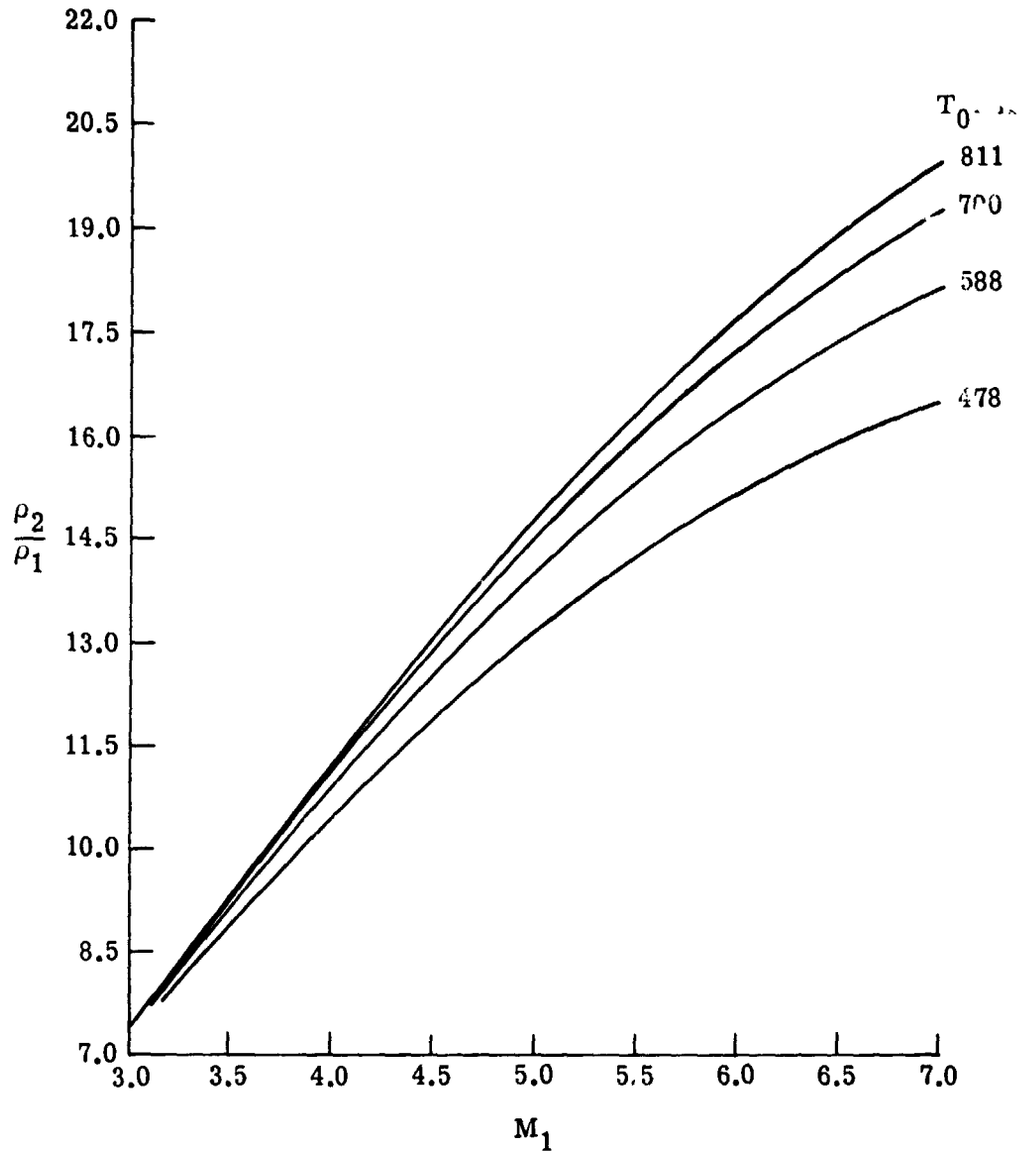

Figure 8.- Variation of density ratio across normal shock with Mach number for C_2F_6. (Independent of stagnation pressure from 1034 to 1724 N/cm^2.)

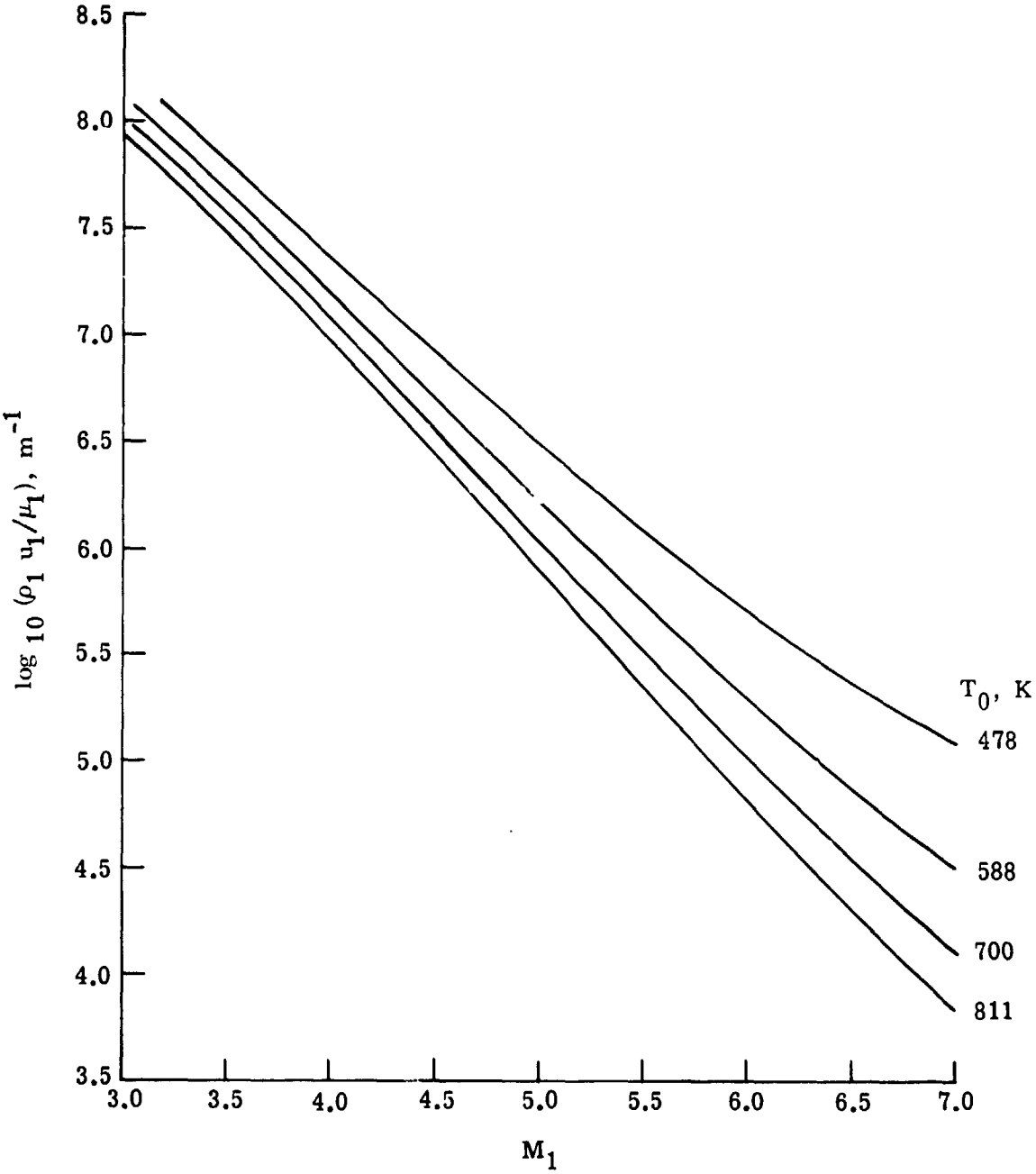

(a) $p_0 = 1034$ N/cm^2.

Figure 9.- Variation of free-stream Reynolds number with Mach number for C_2F_6.

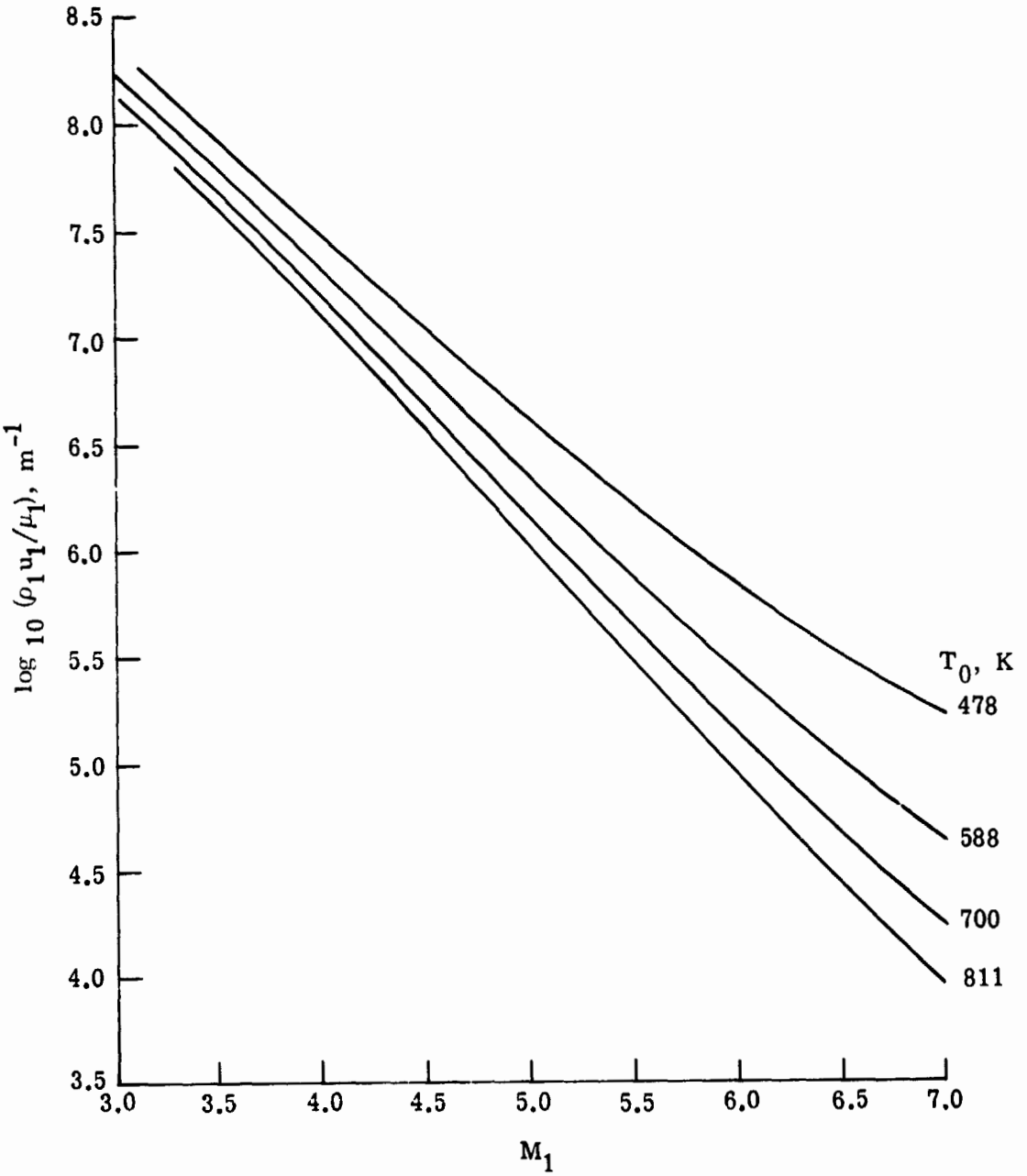

(b) $p_0 = 1378$ N/cm^2.

Figure 9.- Continued.

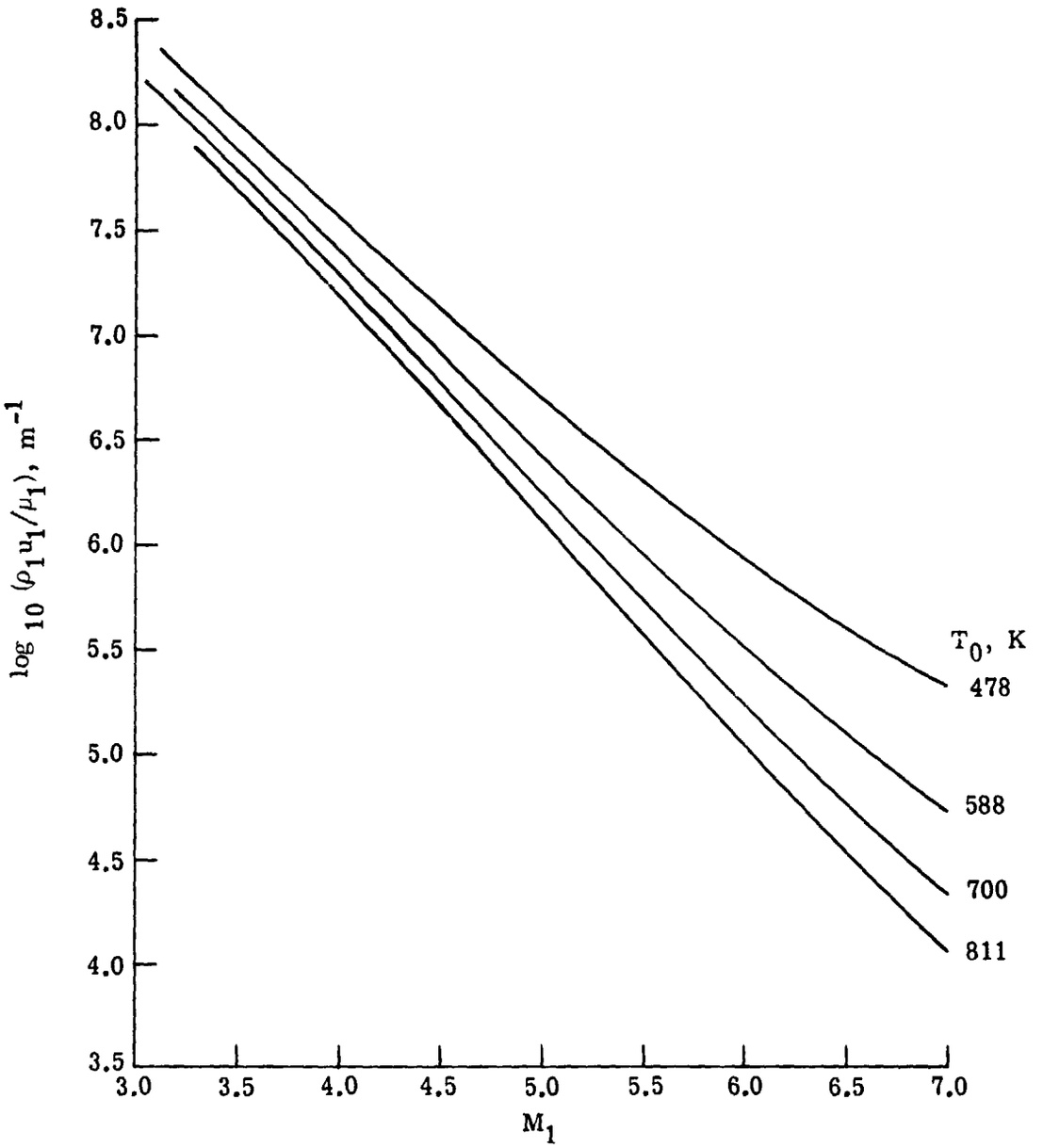

(c) $p_0 = 1724$ N/cm^2.

Figure 9.- Concluded.

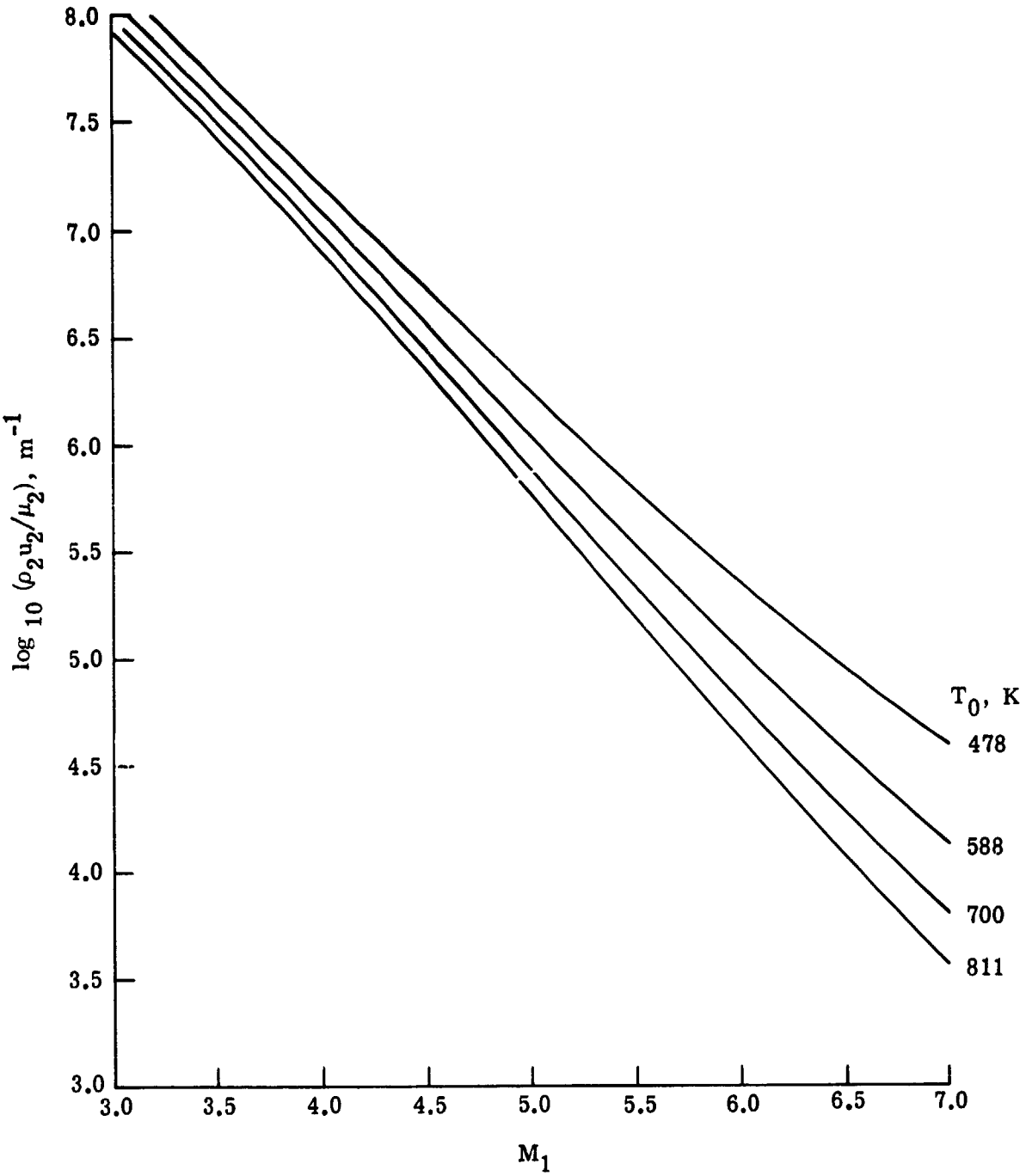

(a) $p_0 = 1034$ N/cm^2.

Figure 10.- Variation of Reynolds number behind normal shock with Mach number for C_2F_6.

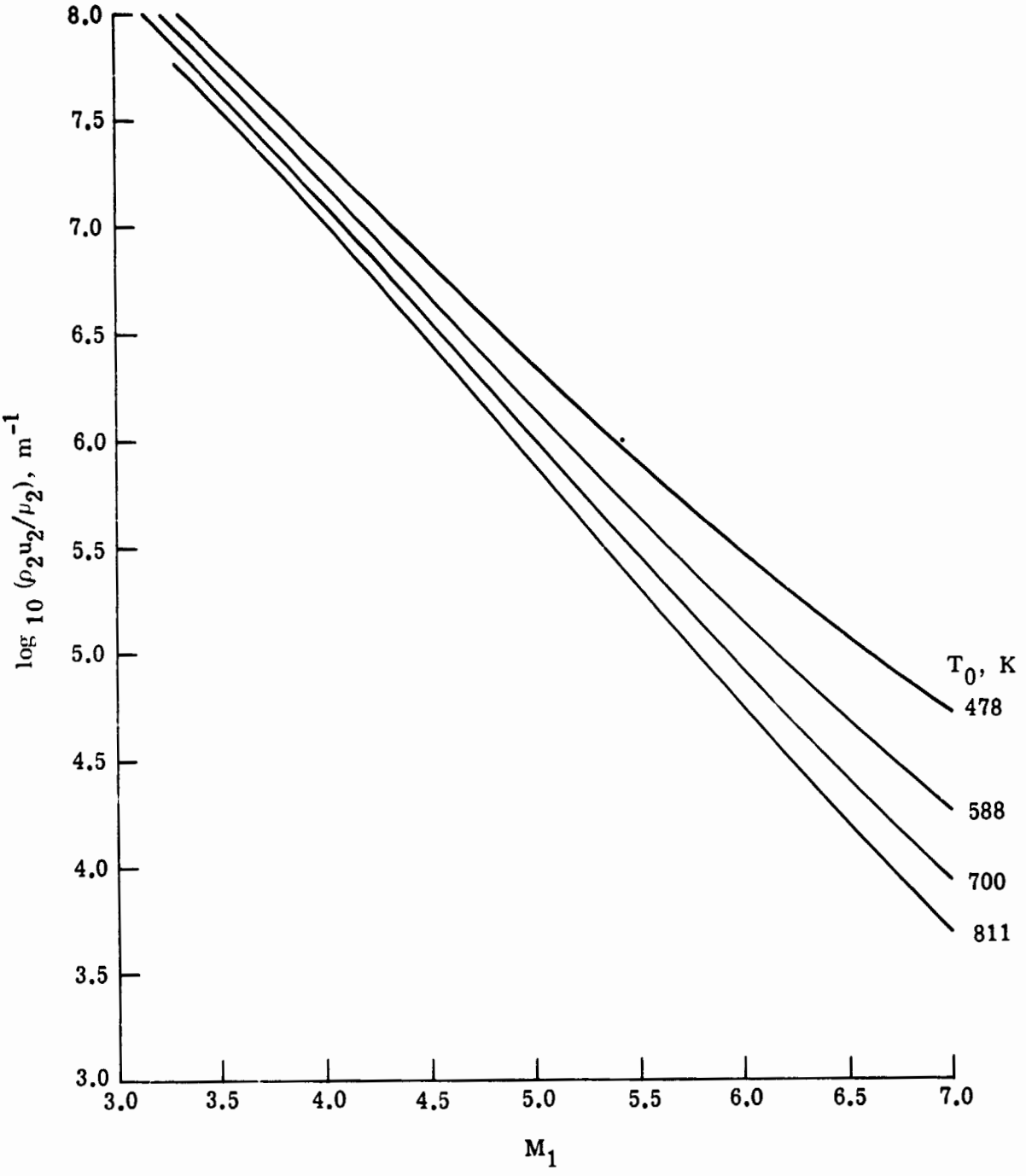

(b) $p_0 = 1378$ N/cm^2.

Figure 10.- Continued.

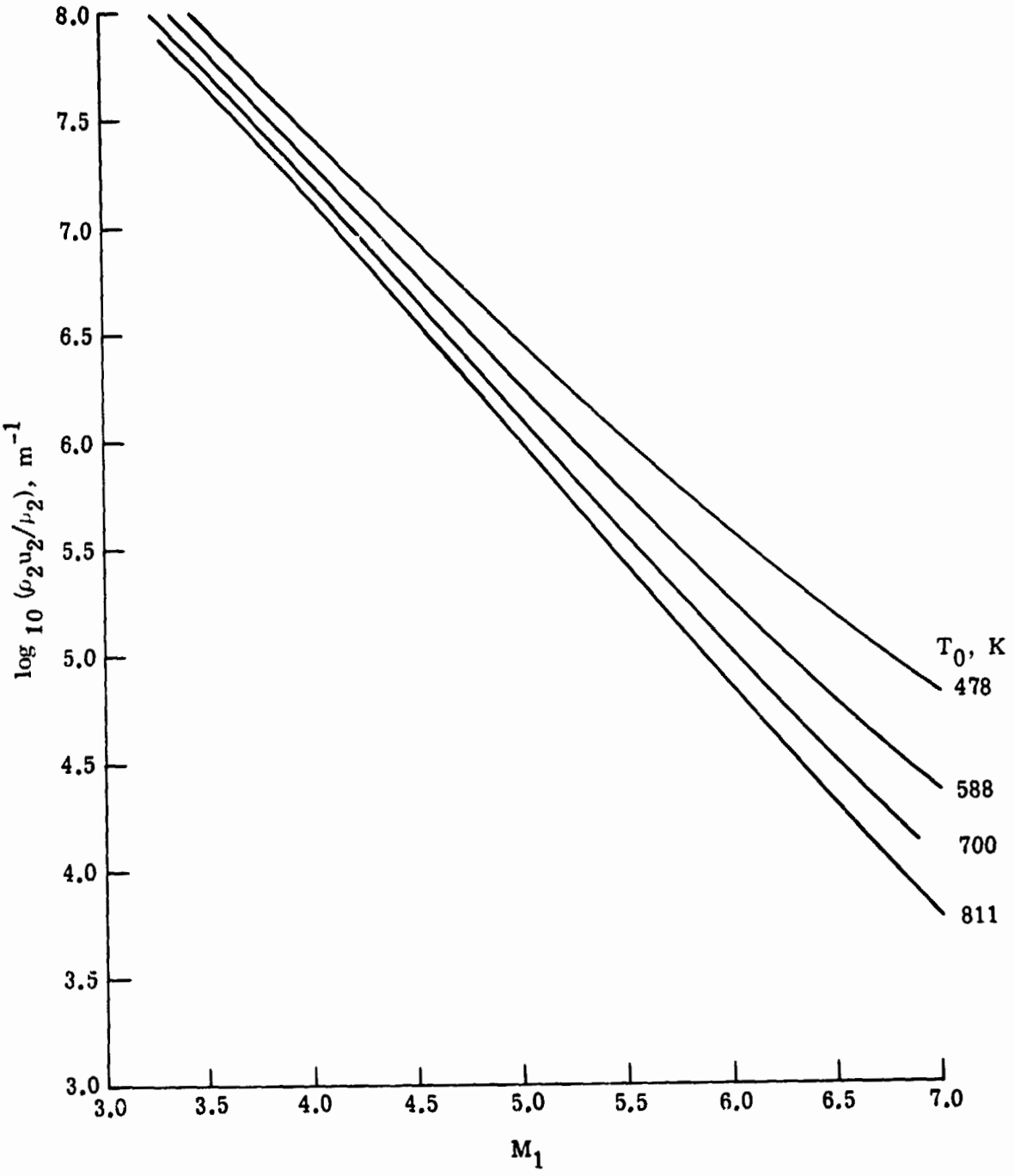

(c) $p_0 = 1724$ N/cm^2.

Figure 10.- Concluded.

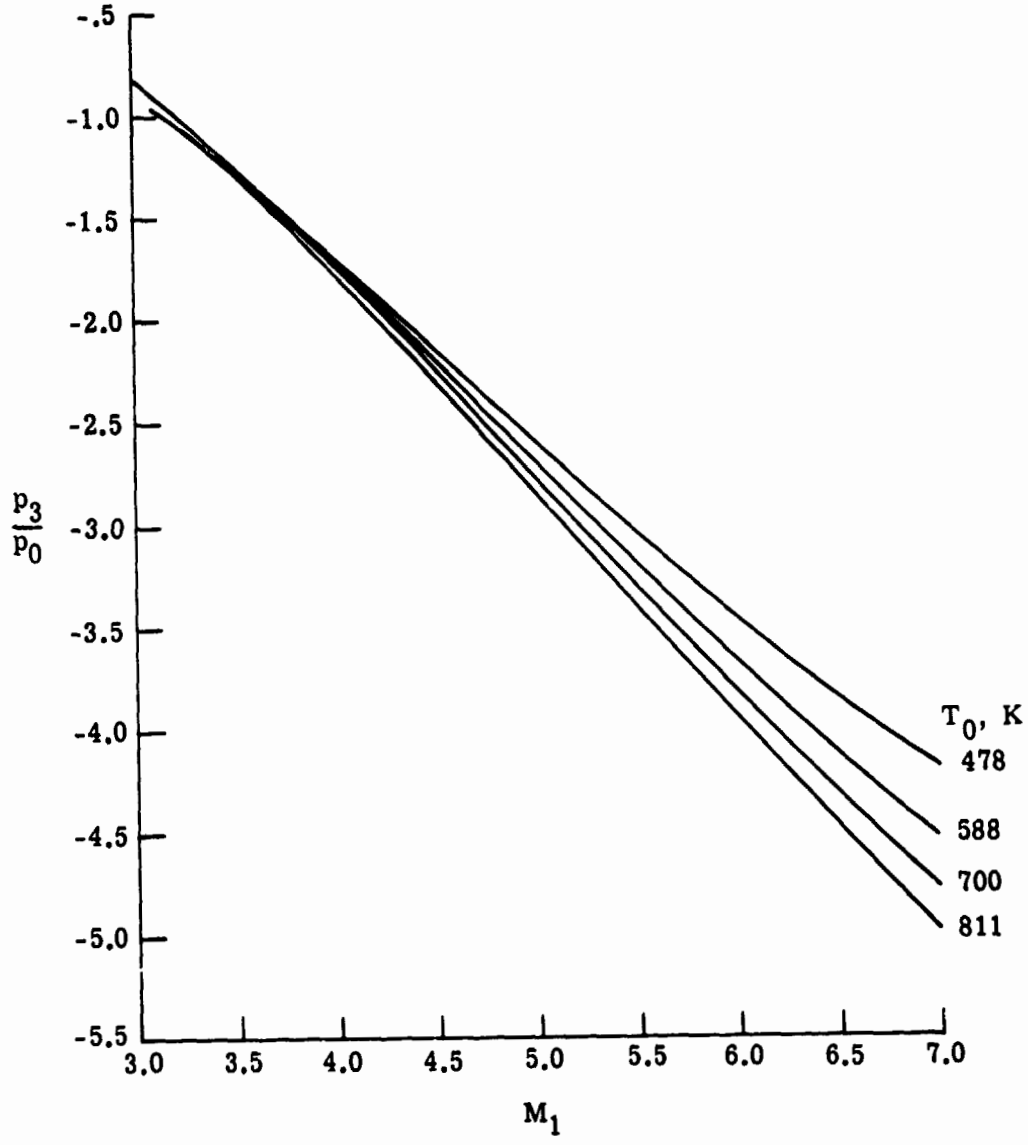

Figure 11.- Variation of ratio of total pressure behind a normal shock to free-stream total pressure with Mach number for C_2F_6. (Independent of stagnation pressure irom 1034 to 1724 N/cm^2.)

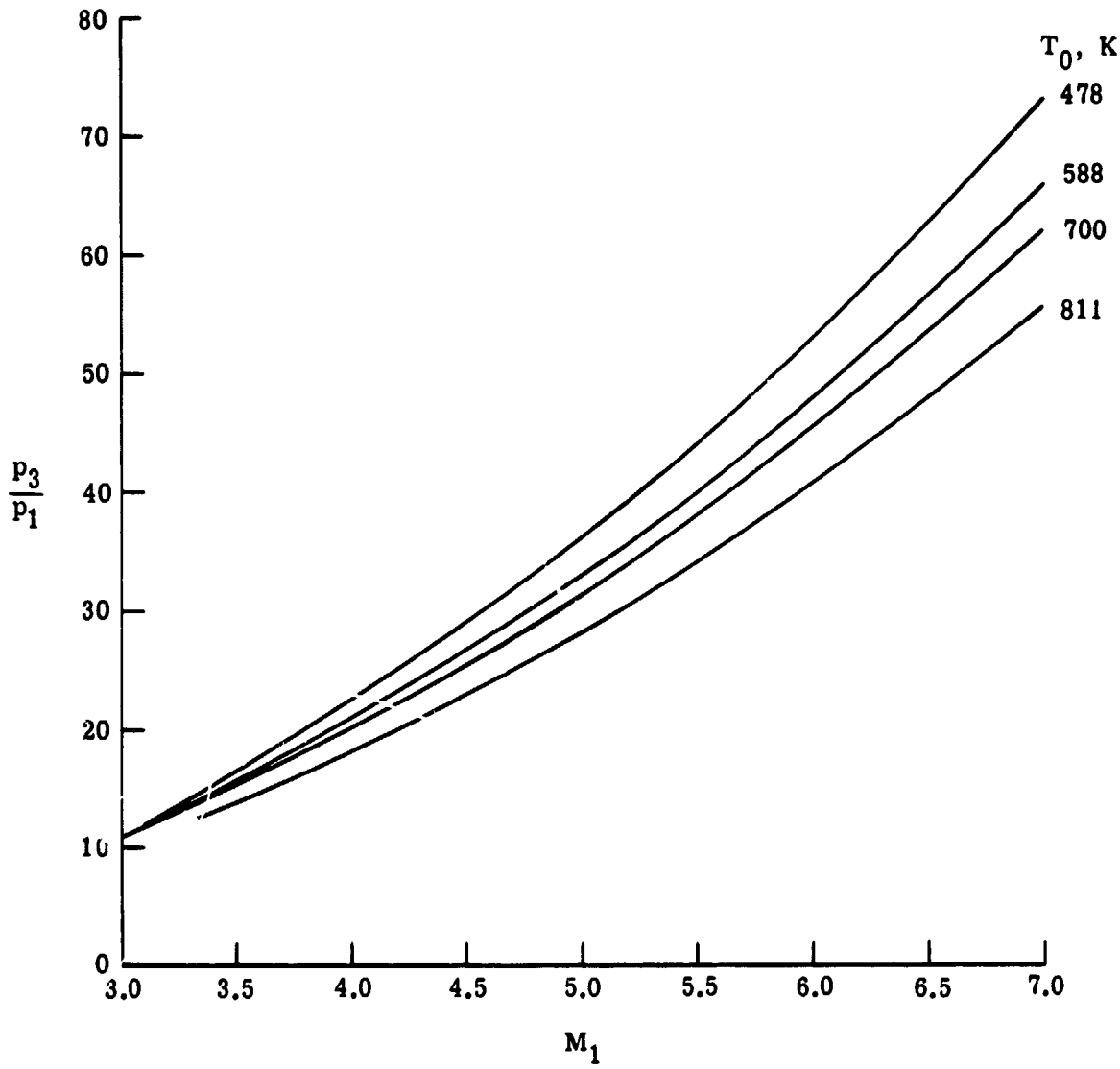

Figure 19 - Variation of ratio of total pressure behind a normal shock to free-stream static pressure with Mach number for C_2F_6. (Independent of stagnation pressure from 1034 to 1724 N/cm^2.)

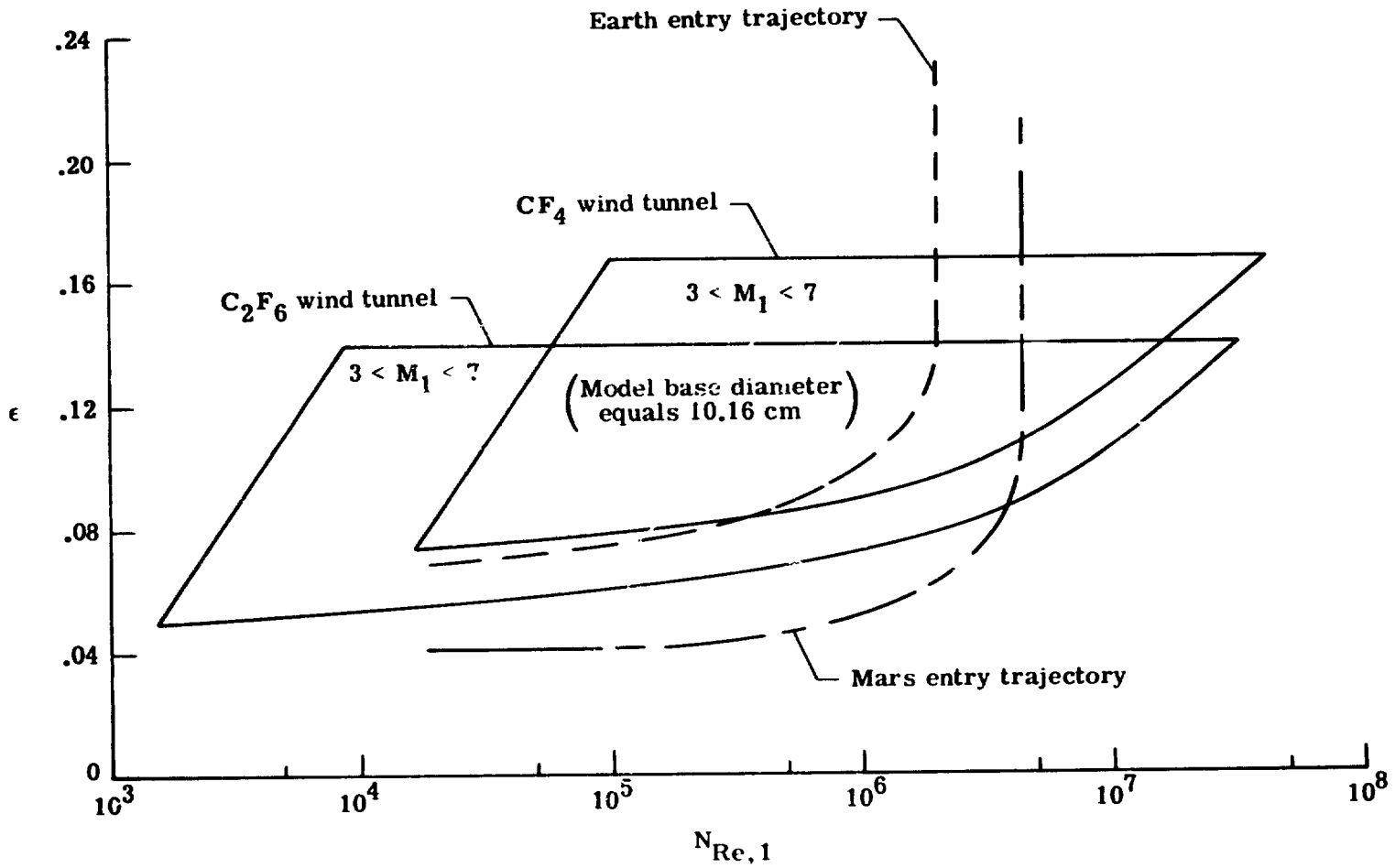

Figure 13.- Capability of obtaining density ratio with C_2F_6 and CF_4.

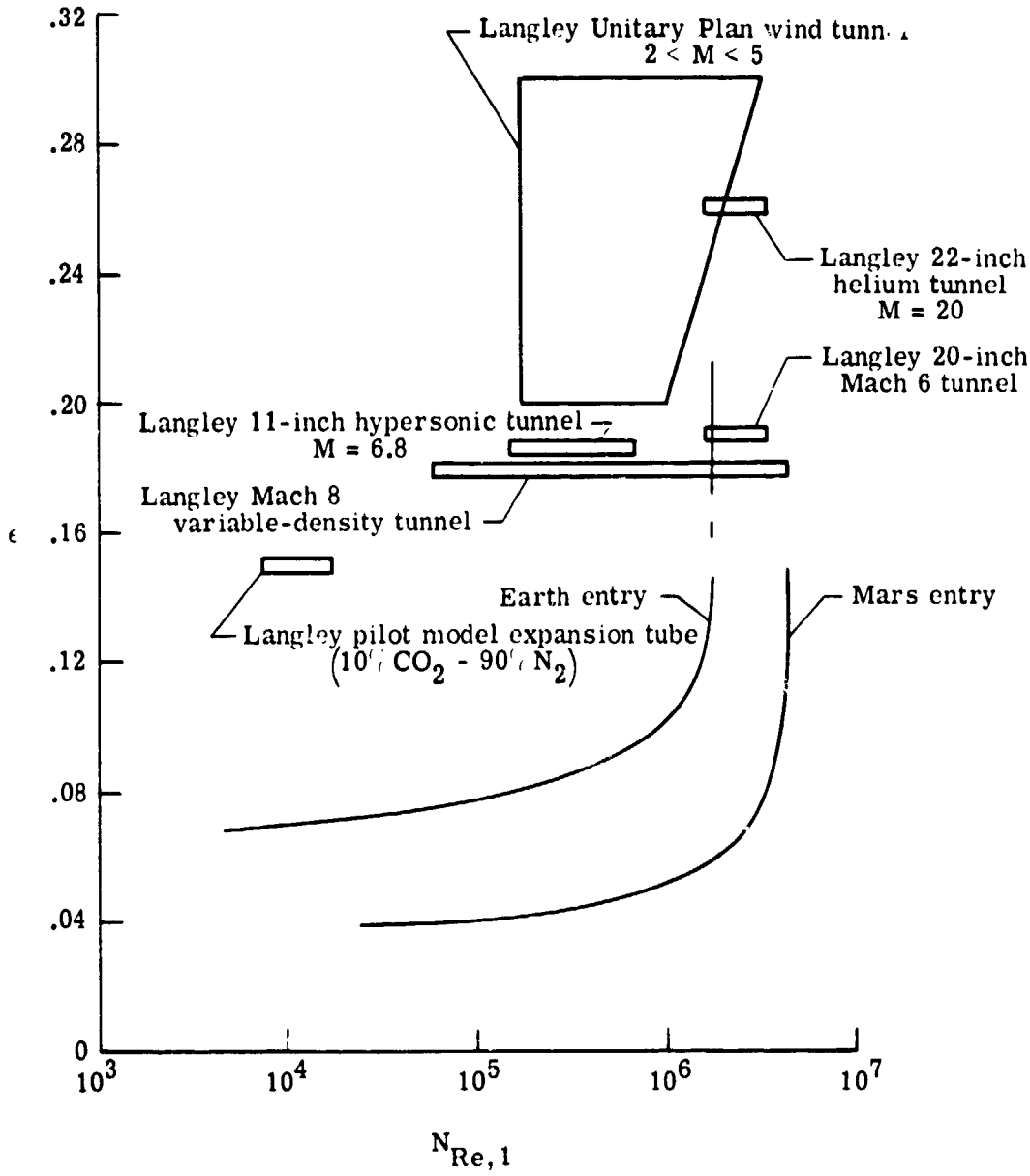

Figure 14.- Density-ratio simulation capability of several facilities.

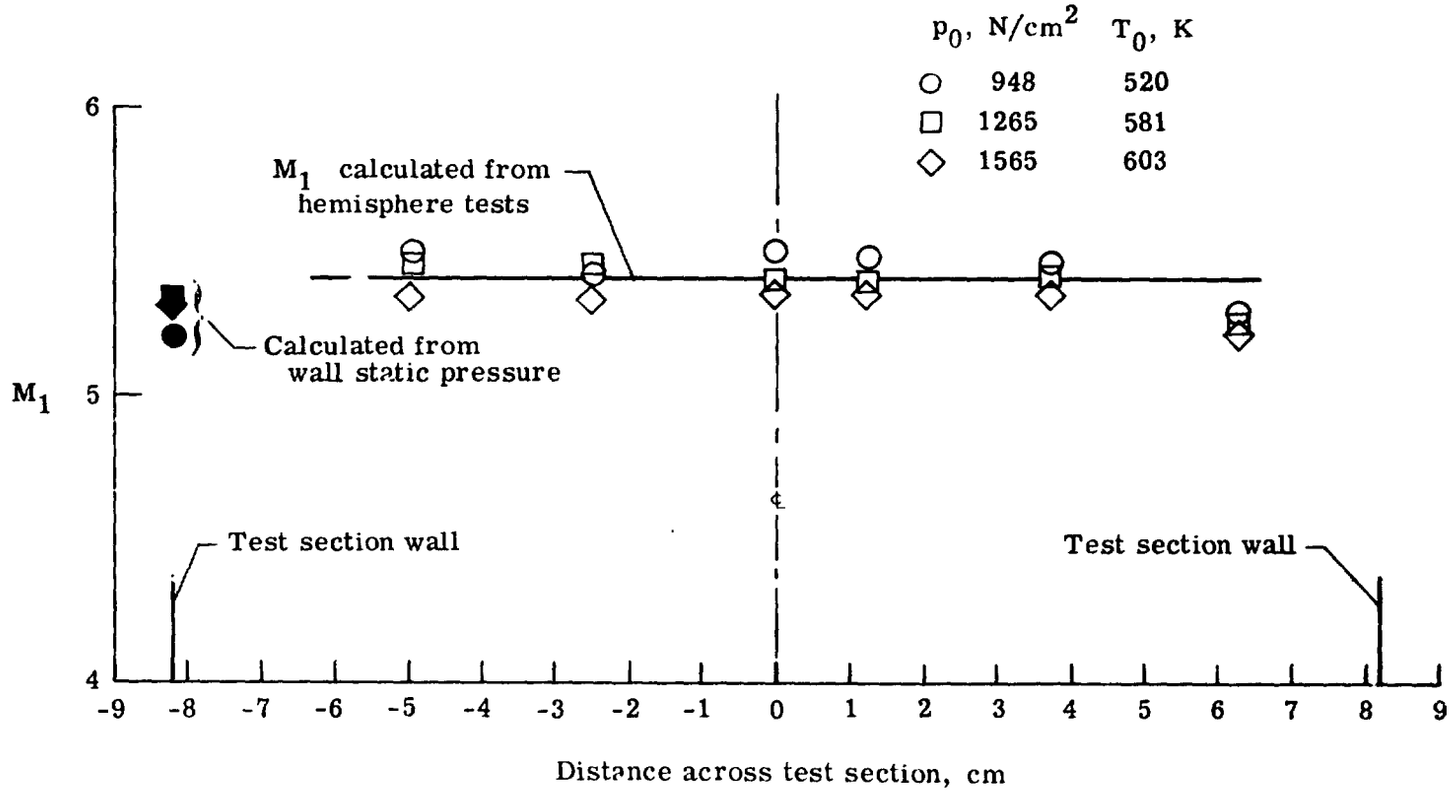

Figure 15.- Mach number distribution in pilot C_2F_6 tunnel (axisymmetric nozzle).

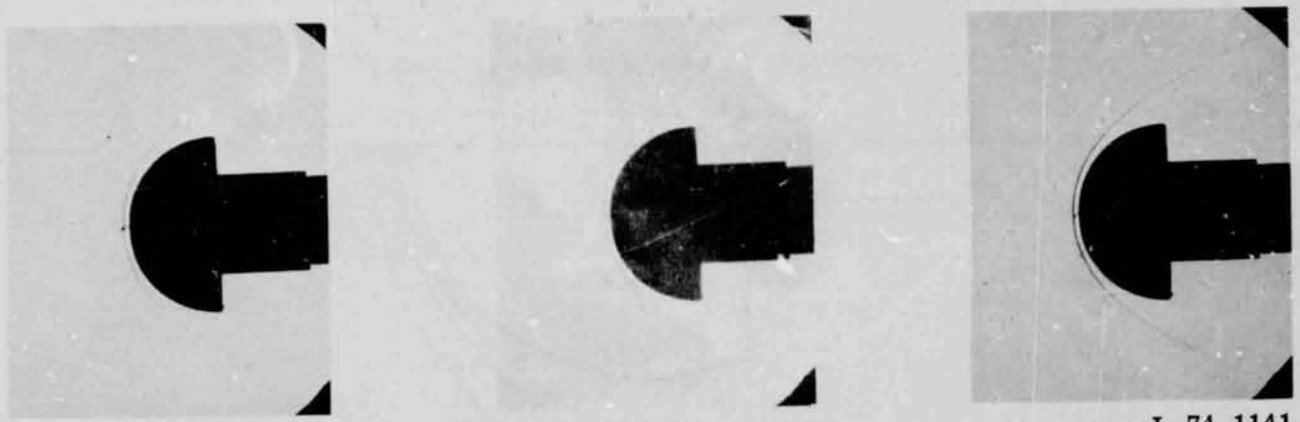

L-74-1141

(a) p_0 = 903 N/cm^2
T_0 = 505 K
$M_{1,cal}$ = 5.40

(b) p_0 = 1250 N/cm^2
T_0 = 580 K
$M_{1,cal}$ = 5.40

(c) p_0 = 1500 N/cm^2
T_0 = 589 K
$M_{1,cal}$ = 5.35

Figure 16.- Shadowgraphs of a 2.54-cm-diameter hemisphere in C_2F_6 pilot tunnel.

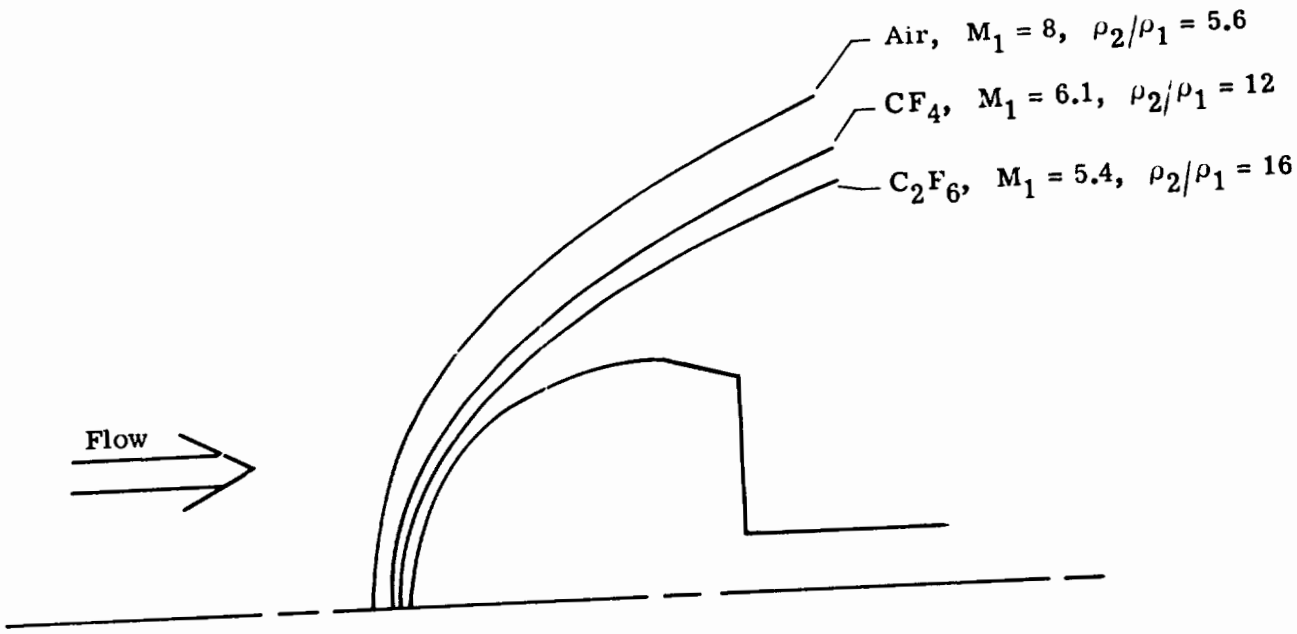

Figure 17.- Shock shapes on hemisphere.

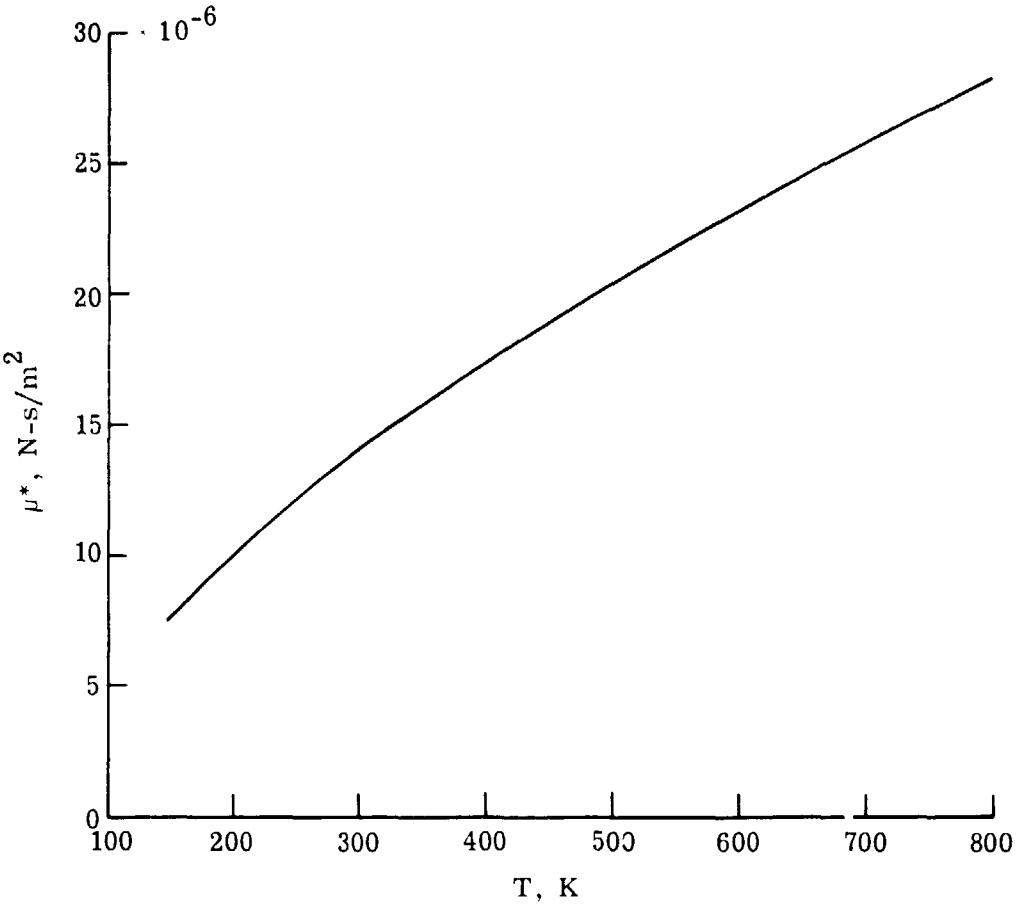

Figure 18.- Viscosity versus temperature; p = 1 atm.

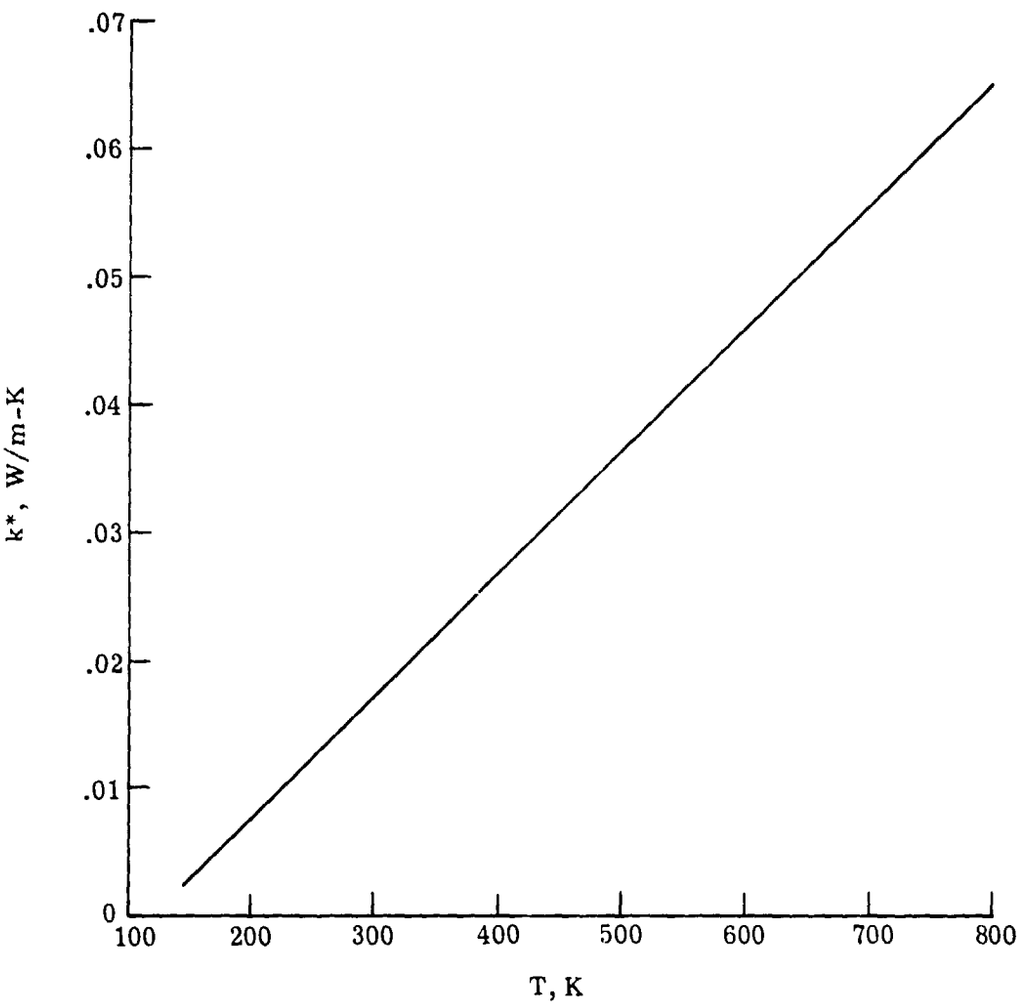

Figure 19.- Thermal conductivity versus temperature; $p = 101.3\ kN/m^2$.

NASA-Langley, 1974 L-9459